

Phonon dispersions and electronic structures of two-dimensional IV-V compounds

Wanxing Lin,^{1,#} Shi-Dong Liang,¹ Jiesen Li,^{2,*} Dao-Xin Yao^{1,†}

¹ State Key Laboratory of Optoelectronic Materials and Technologies, School of Physics, Sun Yat-Sen University, Guangzhou, P. R. China

² School of Environment and Chemical Engineering, Foshan University, Foshan, P. R. China

Present address: # W. L.: Institute of Applied Physics and Materials Engineering, University of Macau, N23 Avenida da Universidade, Taipa, Macau, China

Abstract

One novel family of two-dimensional IV-V compounds have been proposed, whose dynamical stabilities and electronic properties have been systematically investigated using the density functional theory. Extending from our previous work, two phases of carbon phosphorus bilayers α - and β -C₂P₂ have been proposed. Both of them are dynamically stable and thermally stable at 300K. They possess intrinsic HSE gaps of 2.70 eV and 2.67 eV, respectively. Similar α - and β -C₂Y₂ (Y= As, Sb, and Bi) can be obtained if the phosphorus atoms in the α - and β -C₂P₂ replaced by other pnictogens, respectively. If the C atoms in the α - and β -C₂Y₂ (Y= P, As, Sb, and Bi) are further replaced by other IV elements X (X=Si, Ge, Sn, and Pb), respectively, more derivatives of α - and β -X₂Y₂ (Y=N, P, As, Sb, and Bi) also can be obtained. It was found that the majority of them are dynamically stable. The proposed compounds range from metal to insulators depending on their constitutions. All insulated compounds can undergo a transition from insulator to metal induced by biaxial strain. Some of them can undergo a transition from indirect band gap to direct band gap. These new compounds can become candidates as photovoltaic device, thermoelectric material field as well as lamellated superconductors.

Keywords: Two-dimensional, Carbon phosphorus, IV-V compounds, Phonon dispersions, Electronic structures, Biaxial strain

*Corresponding author. E-mail: ljs@fosu.edu.cn (Jiesen Li)

†Corresponding author. E-mail: yaodaox@mail.sysu.edu.cn (Dao-Xin Yao)

Wanxing Lin: 0000-0001-9763-6299.

Shi-Dong Liang: 0000-0001-7753-0024.

Jiesen Li: 0000-0002-5230-2874.

Dao-Xin Yao: 0000-0003-1097-3802.

1. Introduction

Since the discovery of graphene by the mechanical exfoliation in experiment [1], the research on this fantastic two-dimensional (2D) materials has become a focus due to its superior electronic [2] and transport properties [3-5]. Similarly, some other 2D materials comprised of group IV atoms, such as silicene, 2D germanium [6], stanene [7], and plumbene [8, 9], have been proposed theoretically. All of them can exhibit topological properties under certain conditions [7-12], and some phases have been realized in experiment [13-16]. On the other hand, various 2D monolayers comprised of V atoms also have been widely investigated both theoretically [17-20] and experimentally [21-23]. Remarkably, the few-layer phosphorene has an impressive potential application due to its high mobility [24, 25] and novel transport properties [26]. As large tunable bandgap insulators, the nitrogen atomic monolayers [27-31] may be applied in the straintronics field [32]. Following the astonishing superconductivity and correlated property that have been detected in the bilayer twisted graphene [33-39], the investigation of bilayer twisted materials enriched the potential application of 2D materials [40-43].

Besides the exploration of the 2D materials comprised of only one element in group IV or V, various binary compounds also received significant attention in recent years. For example, three phases of carbon nitride bilayers have been introduced in our previous work [44], which exhibit novel electronic and mechanical properties [45, 46]. As the nearest neighbor of nitrogen in group V, the phosphorus can also form various binaries with the carbon. The study on organophosphorus compounds contain both carbon and phosphorus is an active field in material science. The phosphorus-carbon binary compounds, which are referred to as phosphorus carbides (PCs), with various stoichiometries have been studied both experimentally and theoretically [47]. Recently, various 2D carbon-phosphorus (CPs) monolayers have been predicted by the first principle investigations [48-53]. The α -CP, β -CP, and γ -CP are promising 2D materials in optoelectronics as well as electronics [48], and the black phosphorus carbide (α -CP) monolayers is a potential material of gas sensors [54]. Furthermore, the few-layer black carbide phosphorus (α -CP) has a bright application of the field-effect transistor in experiment [55]. The stable phosphorus carbide (β_0 -PC) monolayer [49] can exhibit robust superconducting behavior [56]. It has been found that the P-C bond could enhance the performance of battery anodes [57]. The carbon can also form monolayers with the other elements in group V, the 2D material M_2C_3 ($M = As, Sb, \text{ and } Bi$) with high carrier mobility have potential applications in the photovoltaic field [58].

This work begins with two phases of carbon phosphorus monolayers, named α - C_2P_2 and β - C_2P_2 , respectively. Based on the structures of two monolayers, a family monolayers α - C_2Y_2 and β - C_2Y_2 ($Y = As, Sb, \text{ and } Bi$) have been proposed by replacing the phosphorus atoms with the others in group V. All the α - C_2Y_2 and β - C_2Y_2 ($Y = P, As, Sb, \text{ and } Bi$) have been systematically investigated. These 2D

materials are dynamically stable, and range from insulators to metals, in which the insulators can occur insulator-metal transition under strains. Furthermore, as the C atoms in α - and β -C₂Y₂ (Y = P, As, Sb, and Bi) replaced by the other elements X (X = Si, Ge, Sn, and Pb) in group IV, more monolayers have been proposed, the dynamical stabilities, the thermal stabilities, as well as the electronic properties, have been systematically investigated.

2. Calculation methods

The projector augmented wave and Perdew-Burke-Ernzerhof (PBE) functional exchange-correlation [59] have been used to optimize the crystal structures and calculate the electronic structures, as implemented in the Vienna Ab initio Simulation Package (VASP) code [60]. A screened Coulomb potential has been used in the Heyd-Scuseria-Ernzerhof (HSE06) hybrid functional calculation [61, 62]. A vacuum no less than 20 Å has been inserted to the bilayers to eliminate the coupling between periodic images. The structures have been relaxed until all the components of the net forces on the ions are no more than 10^{-4} eV/Å, and the convergence criterion in the electronic iteration is 10^{-8} eV. The Brillouin zone was sampled by the $20 \times 20 \times 1$ k Γ -centered grid. The phonon dispersions have been calculated by using VASP + Phonopy based on the finite displacement method [63]. The *ab initio* molecular dynamics (AIMD) simulations were based on the Nosé thermostat for 5 ps with a time step of 1 femtosecond [64]. Similar to the C₂N₂ system [45], the canonical ensemble (NVT) system of (6×6) hexagonal supercell includes 144 atoms sampled on the (1×1×1) grid mesh that were simulated. The cut-off energy and the size of the supercells for calculations of the force constants are available in Table S9 of the Supplementary Material (SM).

3. Results and discussion

Enlightened by the previously predicated carbon nitride bilayers [44], we proposed two types of carbon phosphorus (C₂P₂) bilayers in this work. As the N atoms in the α - and β -C₂N₂ replaced by the P atoms, two similar bilayers can be obtained, named α -C₂P₂ and β -C₂P₂, respectively. The lattice structures of the 2D materials in the equilibrium state are shown in Fig. 1(a and b), which are consisted of two carbon phosphorus monolayers through the C-C bonds. Both phases are hexagonal structures with the same crystal lattice parameters, the lattice constants a , the length of interlayer C-P band l_{C-P} , and the thickness δ of them are 2.90 Å, 1.89 Å, and 3.30 Å, respectively, which are larger than the α - and β -C₂N₂ [44], as shown in Table 1. While the length of C-C bonds l_{C-C} between layers is 1.55 Å, which is shorter than the C₂N₂ bilayers, but 0.13 Å longer than C-C bonds in the graphene. Both C-C bonding and C-P bonding are sp³ hybridized. Furthermore, more similar bilayers C₂Y₂ (Y= As, Sb, and Bi) can be obtained as the P atoms in the α - and β -C₂P₂ replaced by the Y (Y=As, Sb, and Bi) atoms in group

V, which have the similar lattice structures and bonding characteristic of C_2P_2 bilayers. The fully optimized crystal lattice parameters of C_2Y_2 ($Y=N, P, As, Sb, \text{ and } Bi$) in Table 1 indicate that as the atomic number of Y ($Y=N, P, As, Sb, \text{ and } Bi$) atom increases, the lattice constant a , the length of interlayer C-Y bond l_{C-Y} , and the thickness of the bilayers δ are monotonously increasing, while the distance between the nearest C atoms l_{C-C} is monotonously decreasing. This trend is consistent with the periodic law of the elements. Similar 2D materials can be obtained if the C atoms in C_2Y_2 ($Y=N, P, As, Sb, \text{ and } Bi$) bilayers are replaced by the group V elements (Si, Ge, Sn, and Pb), which denoted as X_2Y_2 ($X=Si, Ge, Sn, \text{ and } Pb; Y=N, P, As, Sb, \text{ and } Bi$). These derivatives have similar lattice structures and symmetry as α - or β - C_2P_2 , as shown in Fig. 1. The fully optimized crystal lattice parameters of the derivatives are available in Table S1-S4 of the SM. The crystal lattice parameters indicate that, for each particular X ($X=Si, Ge, Sn, \text{ and } Pb$) element, as the atomic number of Y atom increases, the lattice constant a , the X-Y bond length l_{X-Y} , and the thickness of the bilayers δ are monotonously increasing, while the distances between the two nearest atoms in group IV l_{X-X} are monotonously decreasing. All the X_2Y_2 ($X=C, Si, Ge, Sn, \text{ and } Pb; Y=N, P, As, Sb, \text{ and } Bi$) bilayers are hexagonal structures, and the point group of both α and β types are D_{3h} and D_{3d} , respectively. In each layer, the X ($X=C, Si, Ge, Sn, \text{ and } Pb$) atoms and Y ($Y= P, As, Sb, \text{ and } Bi$) atoms are sp^3 hybridized, and thus not coplanar. The Brillouin zone (BZ) of them are regular hexagons, as shown in Fig. 1(c).

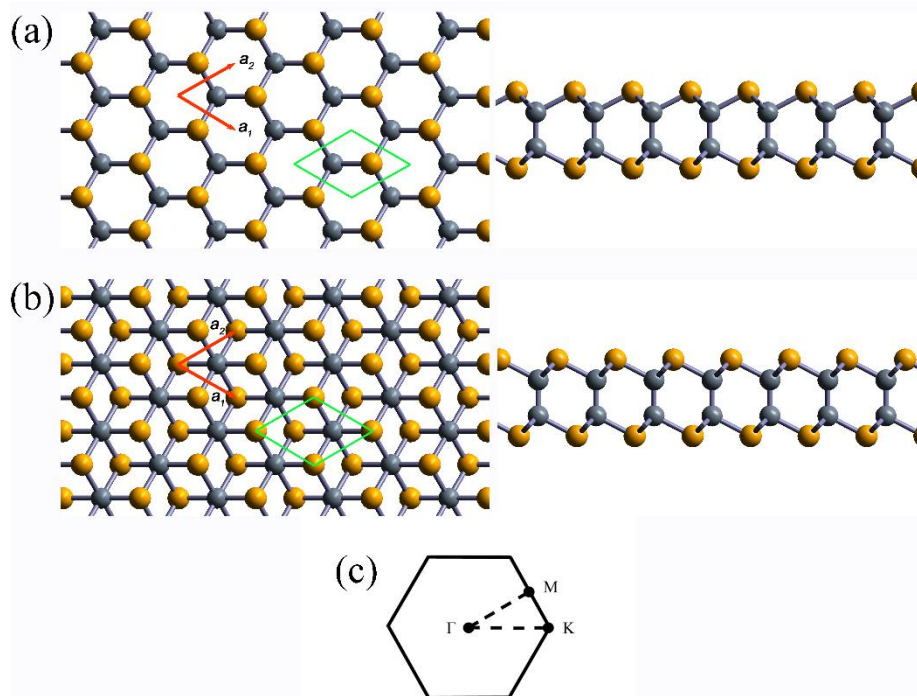


Figure 1. Top view and side view of (a) α - C_2P_2 and (b) β - C_2P_2 bilayer, respectively. The grey and light-yellow spheres denote carbon and phosphorus atoms, respectively. (c) The first Brillouin zone of the two phases.

Table 1. The crystal lattice parameters of C_2Y_2 (Y=N, P, As, Sb, and Bi) (Unit in Å)

Phase	a	l_{c-c}	l_{c-y}	δ
α - C_2N_2 [44]	2.35	1.62	1.44	2.60
β - C_2N_2 [44]	2.35	1.62	1.44	2.60
α - C_2P_2	2.90	1.55	1.89	3.30
β - C_2P_2	2.90	1.55	1.89	3.30
α - C_2As_2	3.11	1.53	2.04	3.46
β - C_2As_2	3.11	1.53	2.04	3.46
α - C_2Sb_2	3.41	1.53	2.25	3.71
β - C_2Sb_2	3.41	1.53	2.25	3.71
α - C_2Bi_2	3.60	1.49	2.38	3.79
β - C_2Bi_2	3.60	1.49	2.38	3.79

To study the dynamical stabilities of all the 46 phases proposed bilayers, their phonon dispersions have been calculated by the first principle theory. The phonon dispersions of the α - and β - C_2Y_2 (Y=P, As, Sb, and Bi) bilayers, as shown in Fig. 2(a-h), exhibit no imaginary frequencies in the BZ. Modes with imaginary frequencies are not oscillatory during their time evolution. This leads to structural instability; in other words, the absence of imaginary frequencies suggests that these materials are dynamically stable [65]. The greater atomic mass of the Y (Y= P, As, Sb, Bi) atoms results in smaller acoustic velocities, higher optical frequencies, and broader frequency gaps. In order to test the evolution of the structures at finite temperature, the AIMD simulation of the α -and β - C_2Y_2 (Y=P, As, Sb, Bi) has been performed for 5 picoseconds at 300 K. The variation of the total energy with time in AIMD simulations at 300 K, and the final geometry structures are available in Figures S1-S8 of the SM. From the final geometry structures, all α -and β - C_2Y_2 (Y=P, As, Sb) as well as β - C_2Bi_2 have not reconstructed or structure damage after 5 picoseconds simulation, which manifests that these structures are stable at 300K. While the α - C_2Bi_2 structure has reconstructed and light structure damage after 5 picoseconds simulation, which indicates this structure may not stand free for a long time at 300K. Furthermore, for α - Si_2P_2 , β - Si_2P_2 , α - Si_2As_2 , β - Si_2As_2 , β - Ge_2P_2 , α - Ge_2As_2 , β - Ge_2As_2 , β - Sn_2N_2 , β - Sn_2P_2 , β - Sn_2As_2 , and α - Sn_2Bi_2 , small imaginary frequency modes are present at the vicinity of Γ . All other derivatives of X_2Y_2 (X=Si, Ge, Sn, and Pb; Y= N, P, As, Sb, and Bi) bilayers are dynamically stable. The phonon dispersions of these materials are available in Figures S9-S27 of the SM. The lowest acoustic modes of α - Pb_2N_2 , β - Pb_2N_2 , α - Pb_2Bi_2 , and β - Pb_2Bi_2 exhibit visible imaginary frequencies around K points or along the Γ -K line in the BZ, as shown in Figure S23 and Figure S27 of the SM, which means these bilayers may not be dynamically stable in the free state. However, we can infer that the β - X_2Y_2 (X=Si, Ge, Sn, and Pb; Y= N, P, As, Sb, and Bi) bilayers are much more stable than the α - X_2Y_2 bilayers at 300K due to the different stacking patterns. Furthermore, we infer that in a particular structure, the smaller mass difference of the two atoms is, the more thermally stable it is.

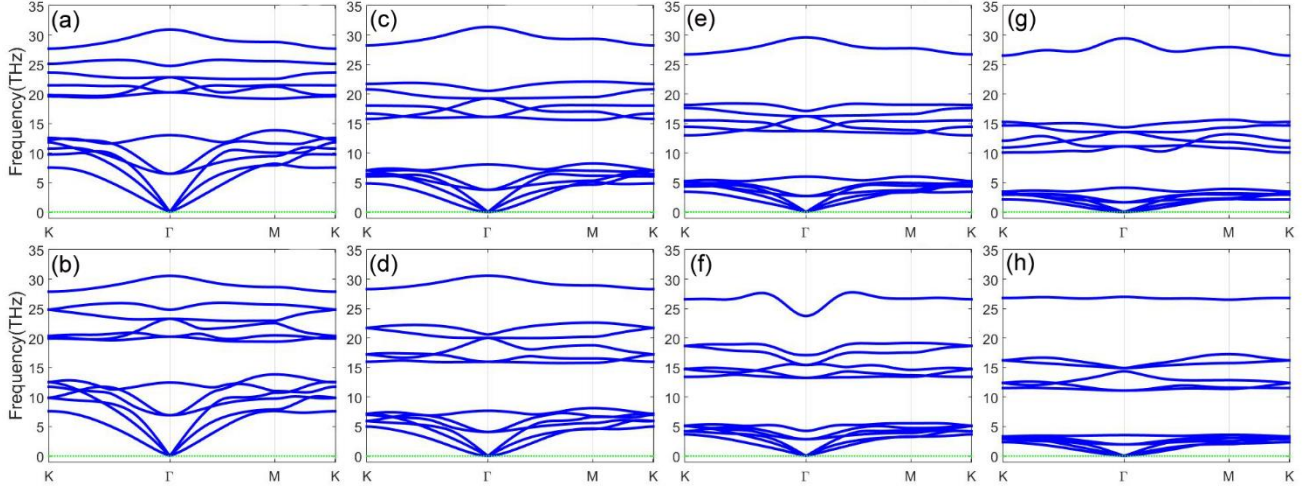


Figure 2. Phonon dispersions of the C_2Y_2 ($Y = P, As, Sb, \text{ and } Bi$) bilayers. (a)~(b) are the phonon dispersions of $\alpha\text{-}C_2P_2$, $\beta\text{-}C_2P_2$, $\alpha\text{-}C_2As_2$, $\beta\text{-}C_2As_2$, $\alpha\text{-}C_2Sb_2$, $\beta\text{-}C_2Sb_2$, $\alpha\text{-}C_2Bi_2$, and $\beta\text{-}C_2Bi_2$, respectively.

The $\alpha\text{-}$ and $\beta\text{-}C_2P_2$ bilayers are indirect insulators with a gap of 1.79 eV and 1.77 eV on the PBE level, respectively, as shown in Fig. 3. On the HSE level, their band gaps become 2.70 eV and 2.67 eV, respectively, which are much narrower than the $\alpha\text{-}$ and $\beta\text{-}C_2N_2$ [44]. The conducting band minimums (CBM) of the $\alpha\text{-}$ and $\beta\text{-}C_2P_2$ at the M and K point in the BZ, respectively. And the valence band maximum (VBM) of both at the Γ points. The spin-orbital coupling (SOC) had not been included in the calculation of $\alpha\text{-}$ and $\beta\text{-}C_2P_2$, while for C_2Y_2 ($Y = As, Sb, \text{ and } Bi$), the SOC have been included in the electronic structure calculations.

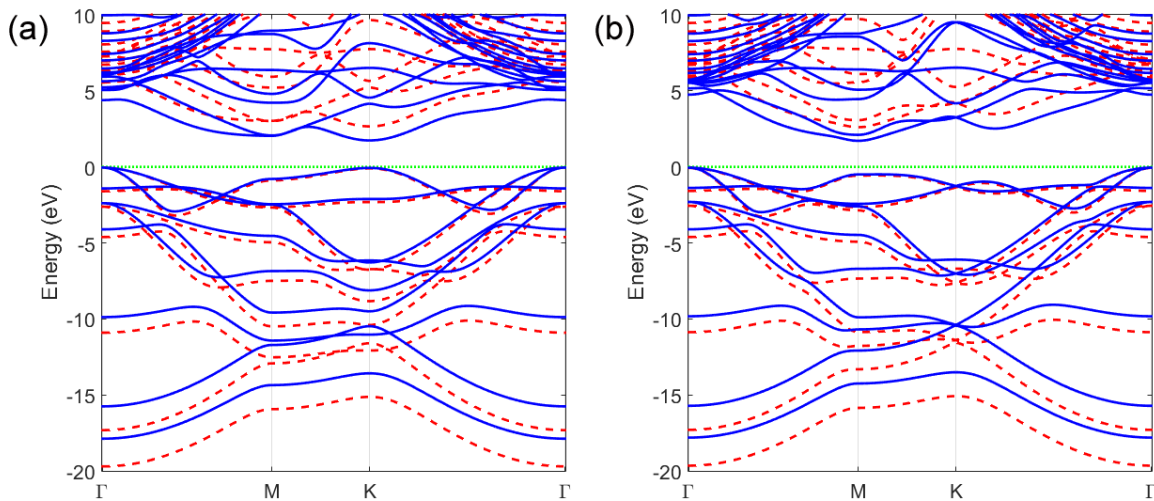


Figure 3. Band structure of $\alpha\text{-}C_2P_2$ (a) and $\beta\text{-}C_2P_2$ (b), the solid blue lines denote results from PBE, and the red dash lines denote results from HSE06.

Even though the PBE method underestimates the band gap of the insulators, the physical properties and the general profile of the proposed materials should be similar. The electronic properties of the other structures are calculated using the PBE method. As shown in Fig. 4(a-c), all the α -C₂As₂, β -C₂As₂, and α -C₂Sb₂ are indirect gap insulators with or without SOC. The calculated gaps of the three phases from PBE are 1.18 eV, 1.02 eV, and 0.22 eV, respectively. And the ones from PBE+SOC calculations are 1.09 eV, 0.95 eV, and 0.07 eV, respectively. As the SOC breaks the degeneracy of the bands in the BZ, the gaps have been decreased by 0.09 eV, 0.07 eV, and 0.15 eV, respectively. The other three phases, β -C₂Sb₂, α -C₂Bi₂, and β -C₂Bi₂, are metals with or without SOC. Interestingly, for both α - and β -C₂Bi₂, there are four crossbands near the Γ points without the SOC, which disappear if the SOC is included. These results imply the possible topological superconductivity under some specific conditions. The values of the bandgaps, the positions of CBM, and VBM are listed in Table 2. From Table 2, we can conclude that for a particular α or β type lattice structure, as the atomic number of group V increases, the band gaps monotonously decrease, while the effect of SOC in the bands increases. Furthermore, the electronic bands of the derivatives X₂Y₂ (X=Si, Ge, Sn, and Pb; Y= N, P, As, Sb, and Bi) also have been calculated, as shown in Fig. S28-S41 of the SM, whose electronic band parameters (the gap value, the CBM, and the VBM positions) listed in Table S5-S8 of the SM.

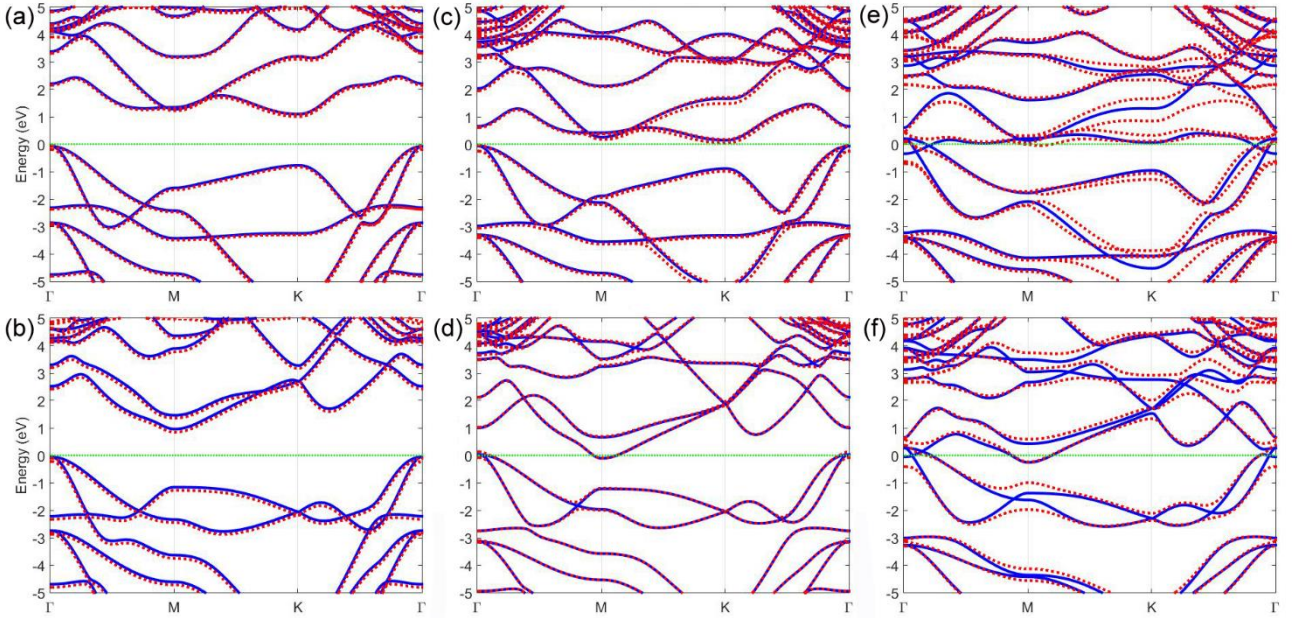


Figure 4. Band structure of (a) α -C₂As₂, (b) β -C₂As₂, (c) α -C₂Sb₂, (d) β -C₂Sb₂, (e) α -C₂Bi₂, (f) β -C₂Bi₂. The blue solid and broken red line curve denotes calculated by PBE and PBE+SOC, respectively.

Table 2. The electronic band parameters of C₂Y₂ (Y=N, P, As, Sb, and Bi) in the PBE background.

Phase	PBE			PBE+SOC			Δ	ε_C (%)
	Gap1 (eV)	CBM position	VBM position	Gap2 (eV)	CBM position	VBM position		
α -C ₂ N ₂	3.76	M	K- Γ	/	/	/	/	27 ^a [44]
β -C ₂ N ₂	4.23	M	K- Γ	/	/	/	/	22 ^a [44]
α -C ₂ P ₂	1.79	K	Γ	/	/	/	/	19 ^a
β -C ₂ P ₂	1.77	M	Γ	/	/	/	/	24 ^a
α -C ₂ As ₂	1.18	K	Γ	1.09	K	Γ	-0.09	14 ^b
β -C ₂ As ₂	1.02	M	Γ	0.95	M	Γ	-0.07	~16 ^b
α -C ₂ Sb ₂	0.22	K	Γ	0.07	K	Γ	-0.15	10 ^b
β -C ₂ Sb ₂	0	M	Γ	0	M	Γ	0	16 ^b
α -C ₂ Bi ₂	0	/	/	0	M-K	Γ	0	/
β -C ₂ Bi ₂	0	/	/	0	M	Γ	0	/

Gap1 and Gap2 represent the band gaps calculated by PBE and PBE+SOC, respectively, $\Delta = \text{Gap2} - \text{Gap1}$. ε_C represents the critical strain from insulativity to metallicity.

a Represents the critical stain in the PBE background.

b Represents the critical stain in the PBE+SOC background.

In the actual applications, the 2D materials are usually attached to the particular substrates, and they are subjected to inevitable lattice mismatch, in which the lattice is either strained or compressed. In other words, the bandgap can be tuned by strain, which is a useful method in the nano materials research field [66-69]. Because the crystal lattices are regular hexagons, the biaxial strain has been applied to tune the bandgap. The strain defined as

$$\varepsilon = \frac{a - a_0}{a_0} \times 100\%$$

where a is the lattice constant under the strain, and a_0 is the lattice constant for the free standing state. As shown in Fig. 6(a), as the biaxial strain increases, both bandgap of α - and β -C₂P₂ monotonically decrease and exhibit linear relations in the range 2-12% and 4-13%, respectively. The gaps of α - and β -C₂P₂ close as the strain reach 19% and 24%, respectively. Because of the realignment of bands in the strain, there are two maxima at 2% and 3-4%, respectively. From the PBE+SOC calculation, the

CBM of α -C₂As₂ locates at the K point in the free state, as shown in Fig. 4(a). As the strain increases, the CBM shifts from K point to Γ point, which changes the indirect gap into a direct one, as shown in Fig. 5(a). The gap will close at strain 14%, if the strain increases further, the conducting band and valence band will cross the Fermi level, as shown in Fig. 5(b). Similar to α -C₂As₂, the CBM of β -C₂As₂ at M points in the free state, as shown in Fig. 4(b). As the strain increases, the CBM shifts from K point to Γ point, which also induces the transition from the indirect gap to a direct gap, as shown in Fig. 5(c). The β -C₂As₂ bilayer will become a gapless semimetal at 16% strain, whose CBM and VBM degenerate at Γ point. Amusingly, the band gap will reopen if the strain increases further, as shown in Fig. 5(d). There are also two maxima at 2% and 6% in the gap-strain relations of α -C₂As₂ and β -C₂As₂, as shown in Fig. 6(b), respectively. The band gaps of α -C₂Sb₂ and β -C₂Sb₂ also close as the strain reach 10% and 16%, respectively. There are two maxima at 2% and 5%, respectively, as shown in Fig. 6(c). Each total energies of the α - and β -C₂Y₂ (Y=P, As, and Sb) monotonically increase as the strain increases, as shown in Fig. 6(d), and the total energy of each β phase is a slightly lower than the α one for any strains. Furthermore, the other insulators, α -Si₂P₂, β -Si₂P₂, α -Si₂As₂, β -Si₂As₂, α -Si₂Sb₂, β -Si₂Sb₂, α -Si₂Bi₂, β -Si₂Bi₂, α -Ge₂N₂, β -Ge₂N₂, α -Ge₂P₂, β -Ge₂P₂, α -Ge₂As₂, β -Ge₂As₂, α -Ge₂Sb₂, β -Ge₂Sb₂, α -Sn₂P₂, β -Sn₂P₂, α -Sn₂As₂, β -Sn₂As₂, α -Sn₂Sb₂, β -Sn₂Sb₂, α -Pb₂P₂, β -Pb₂P₂, α -Pb₂As₂, and β -Pb₂As₂ also can undergo insulator-metal transition by the biaxial strain, as shown in Figure S47-S59 of the SM, and the critical strains of the bilayers listed in Table S5-S8 of the SM.

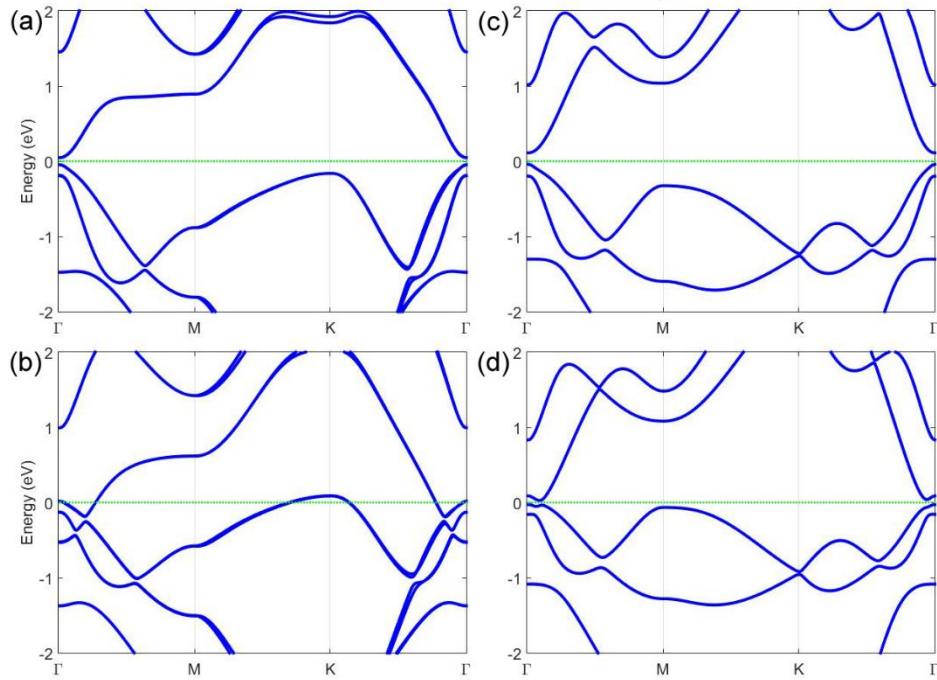


Figure 5. Band structure of α -C₂As₂ under the strain of (a) 12% and (b) 18%, β -C₂As₂ under the strain of (c) 14%, and (d) 18% calculated by PBE+SOC.

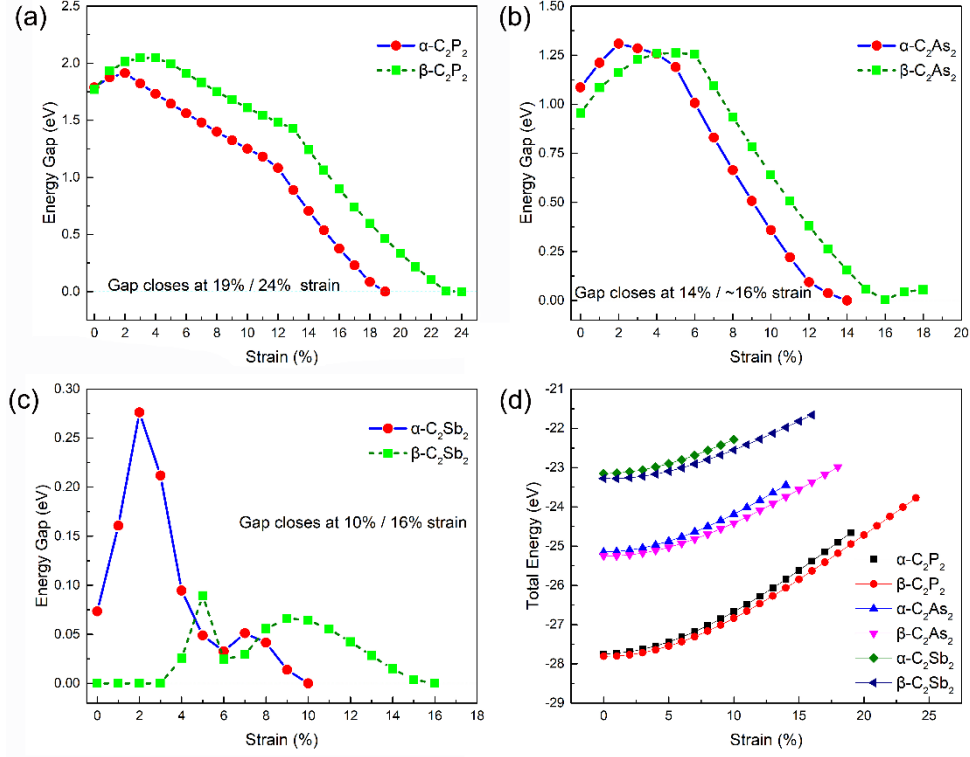


Figure 6. Dependence of energy gaps on the strain of (a) C_2P_2 , (b) C_2As_2 , (c) C_2Sb_2 , and (d) the total energies of them.

4. Conclusions

Forty-six phases of 2D IV-V compounds have been proposed as an extension of our previous work. The dynamical stabilities and electronic properties have been investigated using the density functional theory. The fully optimized structural parameters of the bilayers exhibit trends that are consistent with the periodic law of elements. The phonon dispersions indicate that the majority of the bilayers are dynamically stable in the free state. From the phonon dispersions of the 2D IV-V compounds, one can find that, as the atomic number in the bilayers increases, the highest optical frequency of the phonon decreases. The greater atomic mass of the bilayers implies stronger stability. The AIMD simulations demonstrate that most of the proposed bilayers could be thermally stable even at room temperature. The calculated electronic structures indicate that the bilayers range from insulators to metals with various band gaps, depending on the constitution. Usually, the bilayers containing lighter elements in group IV and lighter elements in group V exhibit broader bandgaps. With a higher atomic number, the SOC effect on the electronic band becomes more significant. For a particular element in group IV, the bilayers own familiar band structures, and the band gap decreases as the atomic number increases. The band gap of the majority bilayers can decrease under strain, even closes, and exhibit transition from insulator to metal. Besides, the band gap of some special bilayers will increase in the beginning, and

then decrease and eventually close under the biaxial strain. The wide-gap bilayers may have potential applications in the photovoltaic devices, and the narrow bandgap ones may become thermoelectric materials. Furthermore, the superconductivity can be investigated by analyzing the electroacoustic coupling effect of the gapless bilayers. In a word, the new 2D materials proposed in this work perhaps become competent candidates in the spintronics and straintronics field. The parallel works of α -C₂P₂ [70] and IV-V compounds [71] have also been reported.

CRedit authorship contribution statement

Wanxing Lin: Conceptualization, Methodology, Validation, Formal analysis, Investigation, Data curation, Writing - original draft, Visualization. **Shi-Dong Liang:** Formal analysis, Resources, Writing - review & editing, Funding acquisition. **Jieshen Li:** Conceptualization, Methodology, Software, Formal analysis, Investigation, Resources, Data curation, Writing - review & editing, Funding acquisition. **Dao-Xin Yao:** Conceptualization, Formal analysis, Resources, Data curation, Writing - review & editing, Supervision, Project administration, Funding acquisition.

Declaration of competing interest

The authors declare that they have no known competing financial interests or personal relationships that could have appeared to influence the work reported in this paper.

Acknowledgments

One of the authors Wanxing Lin, would like to thank Hai-Feng Li, Rui-Qin Zhang, Yu-Jun Zhao, Ji-Hai Liao, Peng-Fei Liu, Lufeng Ruan, Matthew J. Lake, and Vincent Meunier for helpful discussions. W.L. and D.X.Y. are supported by the National Key R&D Program of China (2017YFA0206203, 2018YFA0306001), NSFC-11974432, Guangdong Basic and Applied Basic Research Foundation (2019A1515011337), and the Leading Talent Program of Guangdong Special Projects. S.D.L. is supported by the Natural Science Foundation of Guangdong Province (2016A030313313). J. L. is supported by the NSFC-11747108, the Opening Project of Guangdong Province Key Laboratory of Computational Science at the Sun Yat-Sen University (2018015), Opening Project of Guangdong High Performance Computing Society (2017060103), and High-Level Talent Start-Up Research Project of Foshan University (Gg040934). Most calculations in this work were performed on the Tianhe-2 supercomputer with the help of engineers from the National Supercomputer Center in Guangzhou.

References

- [1] K.S. Novoselov, A.K. Geim, S.V. Morozov, D. Jiang, Y. Zhang, S.V. Dubonos, I.V. Grigorieva, A.A. Firsov, Electric Field Effect in Atomically Thin Carbon Films, *Science* 306(5696) (2004) 666.
- [2] A.H. Castro Neto, F. Guinea, N.M.R. Peres, K.S. Novoselov, A.K. Geim, The electronic properties of graphene, *Reviews of Modern Physics* 81(1) (2009) 109-162.
- [3] N.M.R. Peres, Colloquium: The transport properties of graphene: An introduction, *Reviews of Modern Physics* 82(3) (2010) 2673-2700.
- [4] S. Das Sarma, S. Adam, E.H. Hwang, E. Rossi, Electronic transport in two-dimensional graphene, *Reviews of Modern Physics* 83(2) (2011) 407-470.
- [5] S. Adam, E.H. Hwang, V.M. Galitski, S. Das Sarma, A self-consistent theory for graphene transport, *Proceedings of the National Academy of Sciences* 104(47) (2007) 18392.
- [6] S. Cahangirov, M. Topsakal, E. Aktürk, H. Şahin, S. Ciraci, Two- and One-Dimensional Honeycomb Structures of Silicon and Germanium, *Physical Review Letters* 102(23) (2009) 236804.
- [7] Y. Xu, B. Yan, H.-J. Zhang, J. Wang, G. Xu, P. Tang, W. Duan, S.-C. Zhang, Large-Gap Quantum Spin Hall Insulators in Tin Films, *Physical Review Letters* 111(13) (2013) 136804.
- [8] X.-L. Yu, L. Huang, J. Wu, From a normal insulator to a topological insulator in plumbene, *Physical Review B* 95(12) (2017) 125113.
- [9] Y. Li, J. Zhang, B. Zhao, Y. Xue, Z. Yang, Constructive coupling effect of topological states and topological phase transitions in plumbene, *Physical Review B* 99(19) (2019) 195402.
- [10] C.-C. Liu, W. Feng, Y. Yao, Quantum Spin Hall Effect in Silicene and Two-Dimensional Germanium, *Physical Review Letters* 107(7) (2011) 076802.
- [11] L. Chen, C.-C. Liu, B. Feng, X. He, P. Cheng, Z. Ding, S. Meng, Y. Yao, K. Wu, Evidence for Dirac Fermions in a Honeycomb Lattice Based on Silicon, *Physical Review Letters* 109(5) (2012) 056804.
- [12] L. Li, F. Yang, G.J. Ye, Z. Zhang, Z. Zhu, W. Lou, X. Zhou, L. Li, K. Watanabe, T. Taniguchi, K. Chang, Y. Wang, X.H. Chen, Y. Zhang, Quantum Hall effect in black phosphorus two-dimensional electron system, *Nature Nanotechnology* 11(7) (2016) 593-597.
- [13] P. Vogt, P. De Padova, C. Quaresima, J. Avila, E. Frantzeskakis, M.C. Asensio, A. Resta, B. Ealet, G. Le Lay, Silicene: Compelling Experimental Evidence for Graphenelike Two-Dimensional Silicon, *Physical Review Letters* 108(15) (2012) 155501.
- [14] L. Meng, Y. Wang, L. Zhang, S. Du, R. Wu, L. Li, Y. Zhang, G. Li, H. Zhou, W.A. Hofer, H.-J. Gao, Buckled Silicene Formation on Ir(111), *Nano Letters* 13(2) (2013) 685-690.
- [15] L. Li, S.-z. Lu, J. Pan, Z. Qin, Y.-q. Wang, Y. Wang, G.-y. Cao, S. Du, H.-J. Gao, Buckled Germanene Formation on Pt(111), *Advanced Materials* 26(28) (2014) 4820-4824.
- [16] F.-f. Zhu, W.-j. Chen, Y. Xu, C.-l. Gao, D.-d. Guan, C.-h. Liu, D. Qian, S.-C. Zhang, J.-f. Jia, Epitaxial growth of two-dimensional stanene, *Nature Materials* 14(10) (2015) 1020-1025.
- [17] Z. Zhu, D. Tománek, Semiconducting Layered Blue Phosphorus: A Computational Study, *Physical Review Letters* 112(17) (2014) 176802.
- [18] J. Guan, Z. Zhu, D. Tománek, Phase Coexistence and Metal-Insulator Transition in Few-Layer Phosphorene: A Computational Study, *Physical Review Letters* 113(4) (2014) 046804.
- [19] H. Wang, X. Li, Z. Liu, J. Yang, ψ -Phosphorene: a new allotrope of phosphorene, *Physical Chemistry Chemical Physics* 19(3) (2017) 2402-2408.
- [20] S. Kaur, A. Kumar, S. Srivastava, K. Tankeshwar, Electronic structure engineering of various structural phases of phosphorene, *Physical Chemistry Chemical Physics* 18(27) (2016) 18312-18322.
- [21] A. Castellanos-Gomez, L. Vicarelli, E. Prada, J.O. Island, K.L. Narasimha-Acharya, S.I. Blanter, D.J. Groenendijk, M. Buscema, G.A. Steele, J.V. Alvarez, H.W. Zandbergen, J.J. Palacios, H.S.J. van der Zant, Isolation and characterization of few-layer black phosphorus, *2D Materials* 1(2) (2014) 025001.
- [22] J.-P. Xu, J.-Q. Zhang, H. Tian, H. Xu, W. Ho, M. Xie, One-dimensional phosphorus chain and two-dimensional blue phosphorene grown on Au(111) by molecular-beam epitaxy, *Physical Review Materials* 1(6) (2017) 061002.
- [23] J.L. Zhang, S. Zhao, C. Han, Z. Wang, S. Zhong, S. Sun, R. Guo, X. Zhou, C.D. Gu, K.D. Yuan, Z. Li, W. Chen, Epitaxial Growth of Single Layer Blue Phosphorus: A New Phase of Two-Dimensional Phosphorus, *Nano Letters* 16(8) (2016) 4903-4908.
- [24] L. Li, Y. Yu, G.J. Ye, Q. Ge, X. Ou, H. Wu, D. Feng, X.H. Chen, Y. Zhang, Black phosphorus field-effect transistors, *Nature Nanotechnology* 9(5) (2014) 372-377.
- [25] H. Liu, A.T. Neal, Z. Zhu, Z. Luo, X. Xu, D. Tománek, P.D. Ye, Phosphorene: An Unexplored 2D Semiconductor with a High Hole Mobility, *ACS Nano* 8(4) (2014) 4033-4041.

- [26] R.A. Doganov, E.C.T. O'Farrell, S.P. Koenig, Y. Yeo, A. Ziletti, A. Carvalho, D.K. Campbell, D.F. Coker, K. Watanabe, T. Taniguchi, A.H.C. Neto, B. Özyilmaz, Transport properties of pristine few-layer black phosphorus by van der Waals passivation in an inert atmosphere, *Nature Communications* 6(1) (2015) 6647.
- [27] J. Lee, W.-C. Tian, W.-L. Wang, D.-X. Yao, Two-Dimensional Pnictogen Honeycomb Lattice: Structure, On-Site Spin-Orbit Coupling and Spin Polarization, *Scientific Reports* 5(1) (2015) 11512.
- [28] Y. Zhang, J. Lee, W.-L. Wang, D.-X. Yao, Two-dimensional octagon-structure monolayer of nitrogen group elements and the related nano-structures, *Computational Materials Science* 110 (2015) 109-114.
- [29] J.-S. Li, W.-L. Wang, D.-X. Yao, Band Gap Engineering of Two-Dimensional Nitrogene, *Scientific Reports* 6(1) (2016) 34177.
- [30] W. Lin, J. Li, W. Wang, S.-D. Liang, D.-X. Yao, Electronic Structure and Band Gap Engineering of Two-Dimensional Octagon-Nitrogene, *Scientific Reports* 8(1) (2018) 1674.
- [31] P. Li, W. Luo, A new structure of two-dimensional allotropes of group V elements, *Scientific Reports* 6(1) (2016) 25423.
- [32] K. Roy, S. Bandyopadhyay, J. Atulasimha, Hybrid spintronics and straintronics: A magnetic technology for ultra low energy computing and signal processing, *Applied Physics Letters* 99(6) (2011) 063108.
- [33] G. Trambly de Laissardière, D. Mayou, L. Magaud, Localization of Dirac Electrons in Rotated Graphene Bilayers, *Nano Letters* 10(3) (2010) 804-808.
- [34] R. Bistritzer, A.H. MacDonald, Moiré bands in twisted double-layer graphene, *Proceedings of the National Academy of Sciences* 108(30) (2011) 12233.
- [35] T. Ohta, J.T. Robinson, P.J. Feibelman, A. Bostwick, E. Rotenberg, T.E. Beechem, Evidence for Interlayer Coupling and Moiré Periodic Potentials in Twisted Bilayer Graphene, *Physical Review Letters* 109(18) (2012) 186807.
- [36] S. Dai, Y. Xiang, D.J. Srolovitz, Twisted Bilayer Graphene: Moiré with a Twist, *Nano Letters* 16(9) (2016) 5923-5927.
- [37] Y. Cao, V. Fatemi, A. Demir, S. Fang, S.L. Tomarken, J.Y. Luo, J.D. Sanchez-Yamagishi, K. Watanabe, T. Taniguchi, E. Kaxiras, R.C. Ashoori, P. Jarillo-Herrero, Correlated insulator behaviour at half-filling in magic-angle graphene superlattices, *Nature* 556(7699) (2018) 80-84.
- [38] Y. Cao, V. Fatemi, S. Fang, K. Watanabe, T. Taniguchi, E. Kaxiras, P. Jarillo-Herrero, Unconventional superconductivity in magic-angle graphene superlattices, *Nature* 556(7699) (2018) 43-50.
- [39] Y. Cao, J.Y. Luo, V. Fatemi, S. Fang, J.D. Sanchez-Yamagishi, K. Watanabe, T. Taniguchi, E. Kaxiras, P. Jarillo-Herrero, Superlattice-Induced Insulating States and Valley-Protected Orbits in Twisted Bilayer Graphene, *Physical Review Letters* 117(11) (2016) 116804.
- [40] G. Chen, A.L. Sharpe, P. Gallagher, I.T. Rosen, E.J. Fox, L. Jiang, B. Lyu, H. Li, K. Watanabe, T. Taniguchi, J. Jung, Z. Shi, D. Goldhaber-Gordon, Y. Zhang, F. Wang, Signatures of tunable superconductivity in a trilayer graphene moiré superlattice, *Nature* 572(7768) (2019) 215-219.
- [41] P. Kang, W.-T. Zhang, V. Michaud-Rioux, X.-H. Kong, C. Hu, G.-H. Yu, H. Guo, Moiré impurities in twisted bilayer black phosphorus: Effects on the carrier mobility, *Physical Review B* 96(19) (2017) 195406.
- [42] G. Chen, L. Jiang, S. Wu, B. Lyu, H. Li, B.L. Chittari, K. Watanabe, T. Taniguchi, Z. Shi, J. Jung, Y. Zhang, F. Wang, Evidence of a gate-tunable Mott insulator in a trilayer graphene moiré superlattice, *Nature Physics* 15(3) (2019) 237-241.
- [43] G. Chen, A.L. Sharpe, E.J. Fox, Y.-H. Zhang, S. Wang, L. Jiang, B. Lyu, H. Li, K. Watanabe, T. Taniguchi, Z. Shi, T. Senthil, D. Goldhaber-Gordon, Y. Zhang, F. Wang, Tunable correlated Chern insulator and ferromagnetism in a moiré superlattice, *Nature* 579(7797) (2020) 56-61.
- [44] W. Lin, S.-D. Liang, C. He, W. Xie, H. He, Q. Mai, J. Li, D.-X. Yao, Stabilities and novel electronic structures of three carbon nitride bilayers, *Scientific Reports* 9(1) (2019) 1025.
- [45] Y. Dong, C. Zhang, M. Meng, M.M. Groves, J. Lin, Novel two-dimensional diamond like carbon nitrides with extraordinary elasticity and thermal conductivity, *Carbon* 138 (2018) 319-324.
- [46] R. Longinhos, J. Ribeiro-Soares, Superior stiffness and vibrational spectroscopic signature of two-dimensional diamond-like carbon nitrides, *Physica E: Low-dimensional Systems and Nanostructures* 119 (2020) 114007.
- [47] F. Claeysens, G.M. Fuge, N.L. Allan, P.W. May, S.R.J. Pearce, M.N.R. Ashfold, Phosphorus carbide thin films: experiment and theory, *Applied Physics A* 79(4) (2004) 1237-1241.
- [48] G. Wang, R. Pandey, S.P. Karna, Carbon phosphide monolayers with superior carrier mobility, *Nanoscale* 8(16) (2016) 8819-8825.
- [49] B. Rajbanshi, P. Sarkar, Is the Metallic Phosphorus Carbide (β 0-PC) Monolayer Stable? An Answer from a Theoretical Perspective, *The Journal of Physical Chemistry Letters* 8(4) (2017) 747-754.
- [50] X. Fu, Y. Xie, Y. Chen, Predicting two-dimensional carbon phosphide compounds: C2P4 by the global optimization method, *Computational Materials Science* 144 (2018) 70-75.
- [51] S. Huang, Y. Xie, C. Zhong, Y. Chen, Double Kagome Bands in a Two-Dimensional Phosphorus Carbide P2C3, *The Journal of Physical Chemistry Letters* 9(11) (2018) 2751-2756.

- [52] J. Guan, D. Liu, Z. Zhu, D. Tománek, Two-Dimensional Phosphorus Carbide: Competition between sp^2 and sp^3 Bonding, *Nano Letters* 16(5) (2016) 3247-3252.
- [53] E.R. Heller, J.-O. Joswig, T. Lorenz, G. Seifert, Two-Dimensional Phosphorus Carbide Polymorphs: Influence of Structural Motifs on the Band Gap, *physica status solidi (b)* 255(10) (2018) 1800192.
- [54] J. Zhang, G. Yang, D. Yuan, J. Tian, D. Ma, A first-principles study of doped black phosphorus carbide monolayers as NO_2 and NH_3 sensors, *Journal of Applied Physics* 125(7) (2019) 074501.
- [55] W.C. Tan, Y. Cai, R.J. Ng, L. Huang, X. Feng, G. Zhang, Y.-W. Zhang, C.A. Nijhuis, X. Liu, K.-W. Ang, Few-Layer Black Phosphorus Carbide Field-Effect Transistor via Carbon Doping, *Advanced Materials* 29(24) (2017) 1700503.
- [56] B.-T. Wang, P.-F. Liu, T. Bo, W. Yin, O. Eriksson, J. Zhao, F. Wang, Superconductivity in two-dimensional phosphorus carbide (β 0-PC), *Physical Chemistry Chemical Physics* 20(18) (2018) 12362-12367.
- [57] W. Zhang, J. Yin, P. Zhang, X. Tang, Y. Ding, Two-dimensional phosphorus carbide as a promising anode material for lithium-ion batteries, *Journal of Materials Chemistry A* 6(25) (2018) 12029-12037.
- [58] P.-F. Liu, T. Bo, Z. Liu, O. Eriksson, F. Wang, J. Zhao, B.-T. Wang, Hexagonal M_2C_3 ($M = As, Sb, \text{ and } Bi$) monolayers: new functional materials with desirable band gaps and ultrahigh carrier mobility, *Journal of Materials Chemistry C* 6(46) (2018) 12689-12697.
- [59] J.P. Perdew, K. Burke, M. Ernzerhof, Generalized Gradient Approximation Made Simple, *Physical Review Letters* 77(18) (1996) 3865-3868.
- [60] G. Kresse, J. Furthmüller, Efficient iterative schemes for ab initio total-energy calculations using a plane-wave basis set, *Physical Review B* 54(16) (1996) 11169-11186.
- [61] J. Heyd, G.E. Scuseria, M. Ernzerhof, Hybrid functionals based on a screened Coulomb potential, *The Journal of Chemical Physics* 118(18) (2003) 8207-8215.
- [62] J. Paier, M. Marsman, K. Hummer, G. Kresse, I.C. Gerber, J.G. Ángyán, Screened hybrid density functionals applied to solids, *The Journal of Chemical Physics* 124(15) (2006) 154709.
- [63] A. Togo, I. Tanaka, First principles phonon calculations in materials science, *Scripta Materialia* 108 (2015) 1-5.
- [64] S. Nosé, A unified formulation of the constant temperature molecular dynamics methods, *The Journal of Chemical Physics* 81(1) (1984) 511-519.
- [65] M. Lamparski, B. Van Troeye, V. Meunier, Soliton signature in the phonon spectrum of twisted bilayer graphene, *2D Materials* 7(2) (2020) 025050.
- [66] A.J. Lu, R.Q. Zhang, S.T. Lee, Stress-induced band gap tuning in $\langle 112 \rangle$ silicon nanowires, *Applied Physics Letters* 91(26) (2007) 263107.
- [67] C. Zhang, A. De Sarkar, R.-Q. Zhang, Strain Induced Band Dispersion Engineering in Si Nanosheets, *The Journal of Physical Chemistry C* 115(48) (2011) 23682-23687.
- [68] R.Q. Zhang, E. Bertran, S.T. Lee, Size dependence of energy gaps in small carbon clusters: the origin of broadband luminescence, *Diamond and Related Materials* 7(11) (1998) 1663-1668.
- [69] A.S. Rodin, A. Carvalho, A.H. Castro Neto, Strain-Induced Gap Modification in Black Phosphorus, *Physical Review Letters* 112(17) (2014) 176801.
- [70] X. Cai, Z. Zhu, W. Yu, C. Niu, J. Wang, B. Wang, X. Li, L. Zhang, R. Zhao, Y. Jia, Stable GaSe-like phosphorus carbide monolayer with tunable electronic and optical properties from ab initio calculations, *Materials* 11(10) (2018) 1937.
- [71] B. Özdamar, G. Özbal, M.N. Çınar, K. Sevim, G. Kurt, B. Kaya, H. Sevinçli, Structural, vibrational, and electronic properties of single-layer hexagonal crystals of group IV and V elements, *Physical Review B* 98(4) (2018) 045431.

Supplementary Material for
Phonon dispersions and electronic structures of two-dimensional IV-V compounds

Wanxing Lin,^{1, #} Shi-Dong Liang,¹ Jiesen Li,^{2, *} Dao-Xin Yao^{1, †}

¹ State Key Laboratory of Optoelectronic Materials and Technologies, School of Physics, Sun Yat-Sen University, Guangzhou, P. R. China

² School of Environment and Chemical Engineering, Foshan University, Foshan, P. R. China

Present address: # W. L.: Institute of Applied Physics and Materials Engineering, University of Macau, N23 Avenida da Universidade, Taipa, Macau, China

*Corresponding author. E-mail: ljs@fosu.edu.cn (Jiesen Li)

†Corresponding author. E-mail: yaodaox@mail.sysu.edu.cn (Dao-Xin Yao)

CONTENTS

I. Crystal lattice parameters	2
II. AIMD simulations	4
III. Phonon dispersions	8
IV. Electronic bands	15
V. Dependence of energy gap on the strain	22
VI. Electronic band parameters	26
VII. Computational details	30
VIII. POSCAR files of the structures	31
References	43

I. Crystal lattice parameters

The lattice constants and the distance between the nearest carbon atoms $l_{\text{Si-Y}}$, the Si-Y bond, and the thick of the bilayers δ can be obtained by fully optimized.

Table S1. Crystal lattice parameters of Si_2Y_2 (Y=N, P, As, Sb, Bi) (Unit in Å)

Phase	a	l_{X-X}	l_{X-Y}	δ
α - Si_2N_2 [1]	2.90	2.43	1.76	3.54
β - Si_2N_2 [1]	2.90	2.43	1.76	3.54
α - Si_2P_2	3.53	2.37	2.28	4.41
β - Si_2P_2	3.53	2.37	2.28	4.41
α - Si_2As_2	3.69	2.36	2.40	4.58
β - Si_2As_2	3.69	2.36	2.40	4.58
α - Si_2Sb_2	4.02	2.36	2.62	4.82
β - Si_2Sb_2	4.02	2.36	2.62	4.82
α - Si_2Bi_2	4.17	2.35	2.73	4.92
β - Si_2Bi_2	4.17	2.35	2.73	4.92

Table S2. Crystal lattice parameters of Ge_2Y_2 (Y=N, P, As, Sb, Bi) (Unit in Å)

Phase	a	l_{X-X}	l_{X-Y}	δ
α - Ge_2N_2	3.10	2.57	1.91	3.90
β - Ge_2N_2	3.10	2.57	1.91	3.90
α - Ge_2P_2	3.66	2.51	2.37	4.65
β - Ge_2P_2	3.66	2.51	2.37	4.65
α - Ge_2As_2	3.82	2.50	2.49	4.80
β - Ge_2As_2	3.82	2.50	2.49	4.80
α - Ge_2Sb_2	4.12	2.50	2.69	5.01
β - Ge_2Sb_2	4.12	2.50	2.69	5.01
α - Ge_2Bi_2	4.26	2.49	2.78	5.09
β - Ge_2Bi_2	4.26	2.49	2.78	5.09

Table S3. Crystal lattice parameters of Sn_2Y_2 (Y=N, P, As, Sb, Bi) (Unit in Å)

Phase	a	l_{X-X}	l_{X-Y}	δ
α - Sn_2N_2	3.42	2.98	2.11	4.44
β - Sn_2N_2	3.42	2.98	2.11	4.44
α - Sn_2P_2	3.95	2.89	2.56	5.22
β - Sn_2P_2	3.95	2.89	2.56	5.22
α - Sn_2As_2	4.09	2.88	2.67	5.36
β - Sn_2As_2	4.09	2.88	2.67	5.36
α - Sn_2Sb_2	4.38	2.87	2.87	5.58
β - Sn_2Sb_2	4.38	2.87	2.87	5.58
α - Sn_2Bi_2	4.51	2.86	2.96	5.66
β - Sn_2Bi_2	4.51	2.86	2.96	5.66

Table S4. Crystal lattice parameters of Pb_2Y_2 (Y=N, P, As, Sb, Bi) (Unit in Å)

Phase	a	l_{X-X}	l_{X-Y}	δ
α - Pb_2N_2	3.64	3.17	2.24	4.75
β - Pb_2N_2	3.64	3.17	2.24	4.75
α - Pb_2P_2	4.12	3.06	2.67	5.49
β - Pb_2P_2	3.64	3.17	2.24	4.75
α - Pb_2As_2	4.25	3.05	2.77	5.62
β - Pb_2As_2	4.25	3.05	2.77	5.62
α - Pb_2Sb_2	4.53	3.04	2.96	5.81
β - Pb_2Sb_2	4.53	3.04	2.96	5.81
α - Pb_2Bi_2	4.63	3.02	3.03	5.89
β - Pb_2Bi_2	4.63	3.02	3.03	5.89

II. AIMD simulations

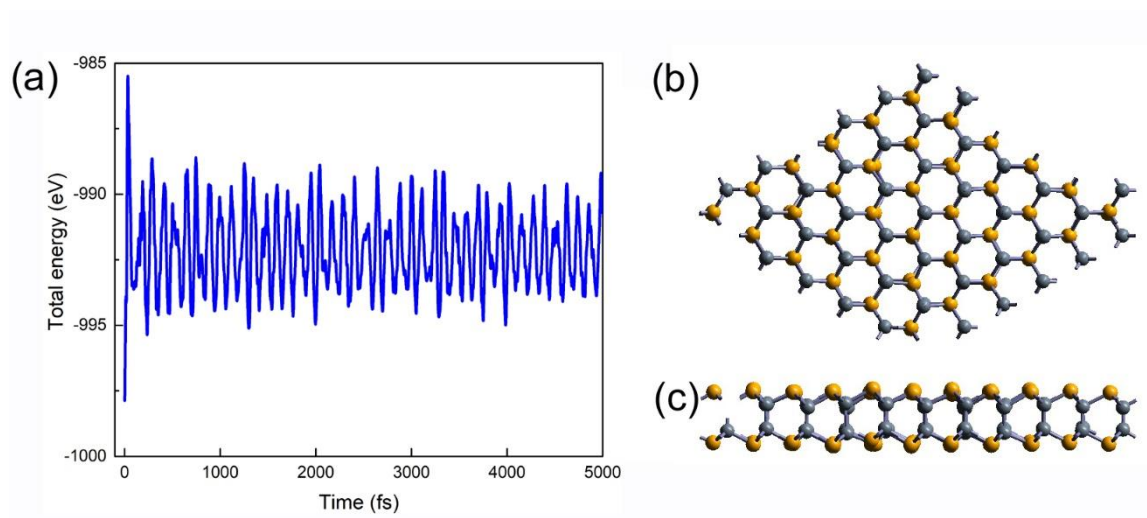


Figure S1. (a) The variation of the total energy of α -C₂P₂ with time in AIMD simulations at 300 K, (b) and (c) show the top view and side view of the final geometry structure, respectively.

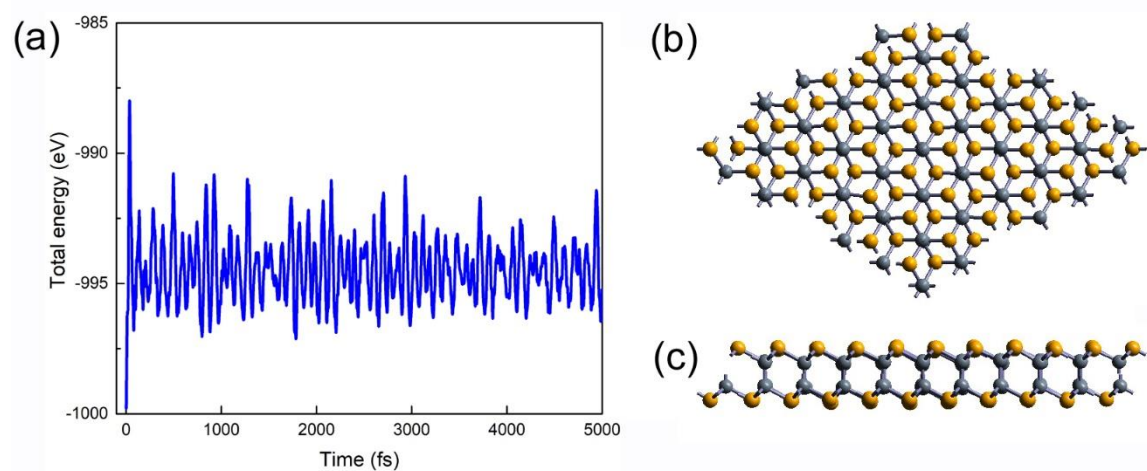


Figure S2. (a) The variation of the total energy of β -C₂P₂ with time in AIMD simulations at 300 K, (b) and (c) show the top view and side view of the final geometry structure, respectively.

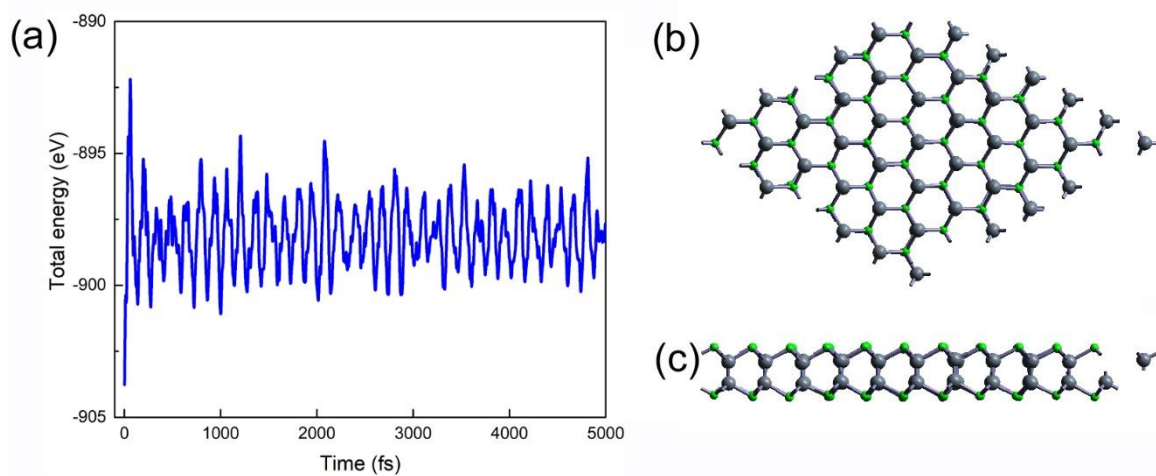


Figure S3. (a) The variation of the total energy of $\alpha\text{-C}_2\text{As}_2$ with time in AIMD simulations at 300 K, (b) and (c) show the top view and side view of the final geometry structure, respectively.

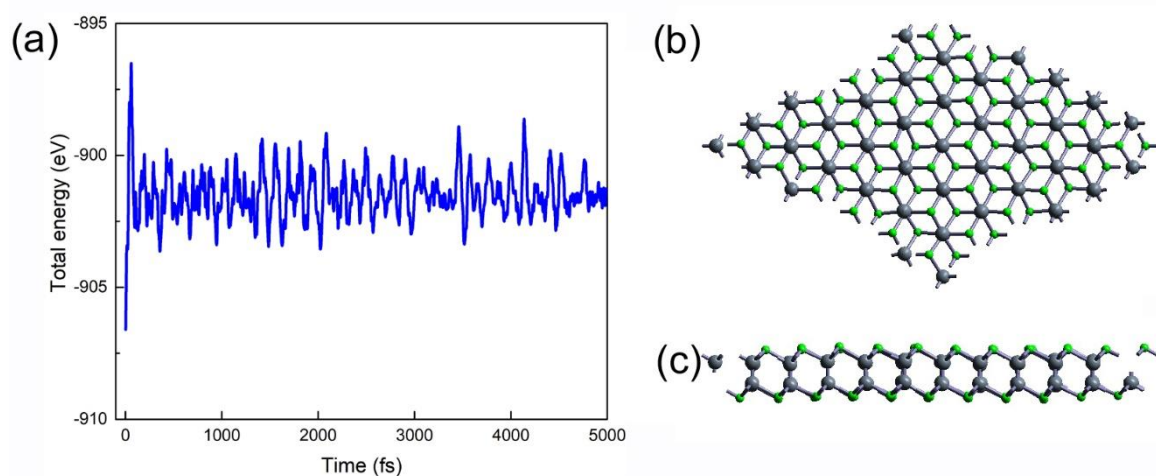


Figure S4. (a) The variation of the total energy of $\beta\text{-C}_2\text{As}_2$ with time in AIMD simulations at 300 K, (b) and (c) show the top view and side view of the final geometry structure, respectively.

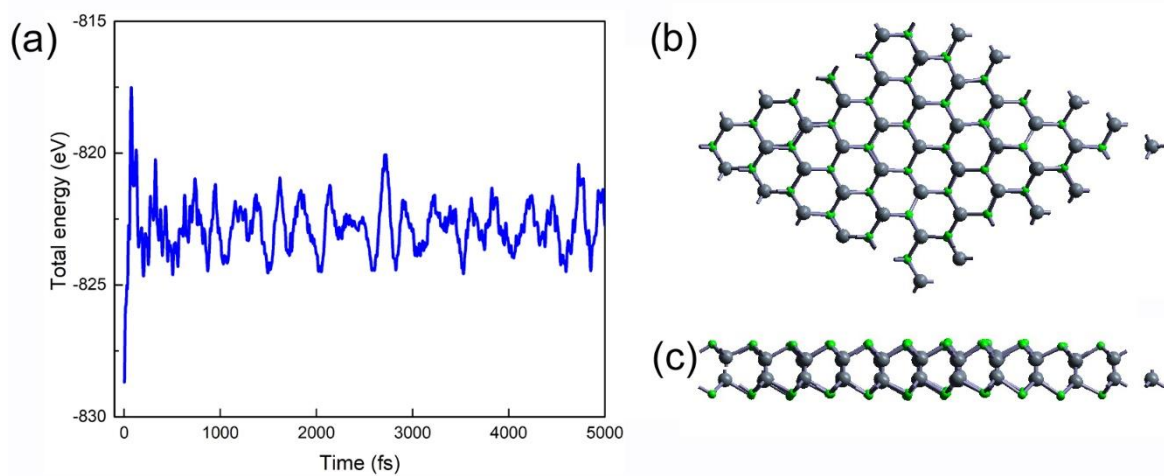


Figure S5. (a) The variation of the total energy of α -C₂Sb₂ with time in AIMD simulations at 300 K, (b) and (c) show the top view and side view of the final geometry structure, respectively.

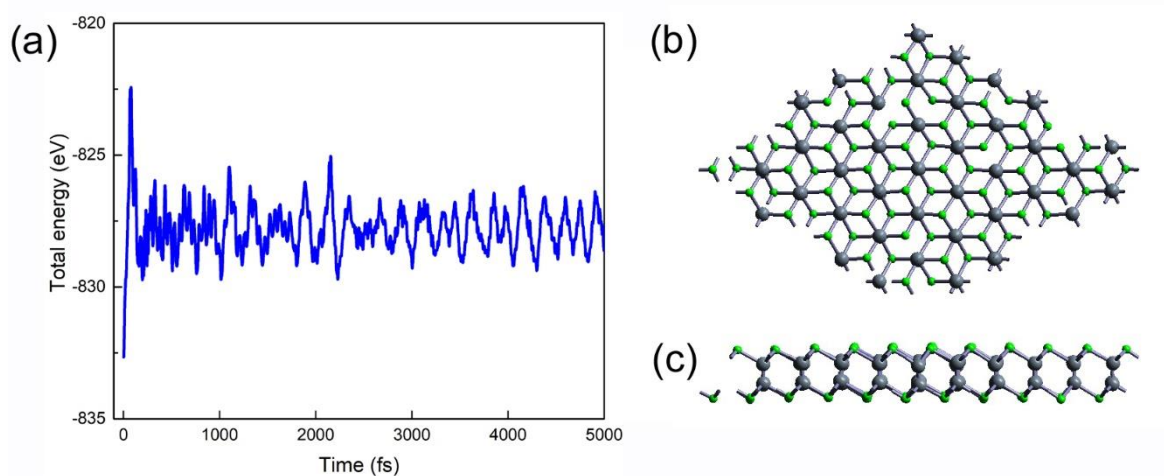


Figure S6. (a) The variation of the total energy of β -C₂Sb₂ with time in AIMD simulations at 300 K, (b) and (c) show the top view and side view of the final geometry structure, respectively.

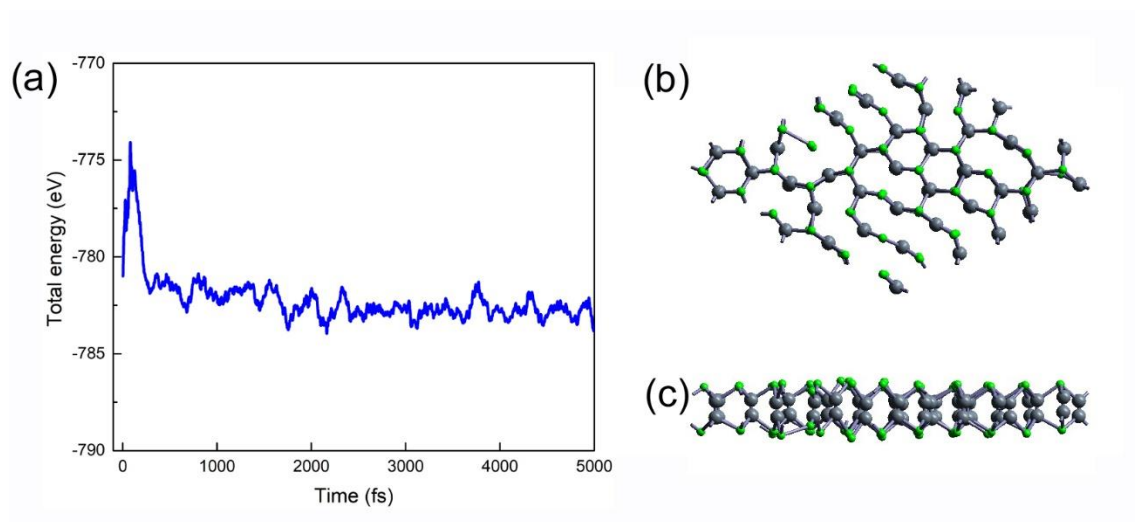


Figure S7. (a) The variation of the total energy of α -C₂Bi₂ with time in AIMD simulations at 300 K, (b) and (c) show the top view and side view of the final geometry structure, respectively.

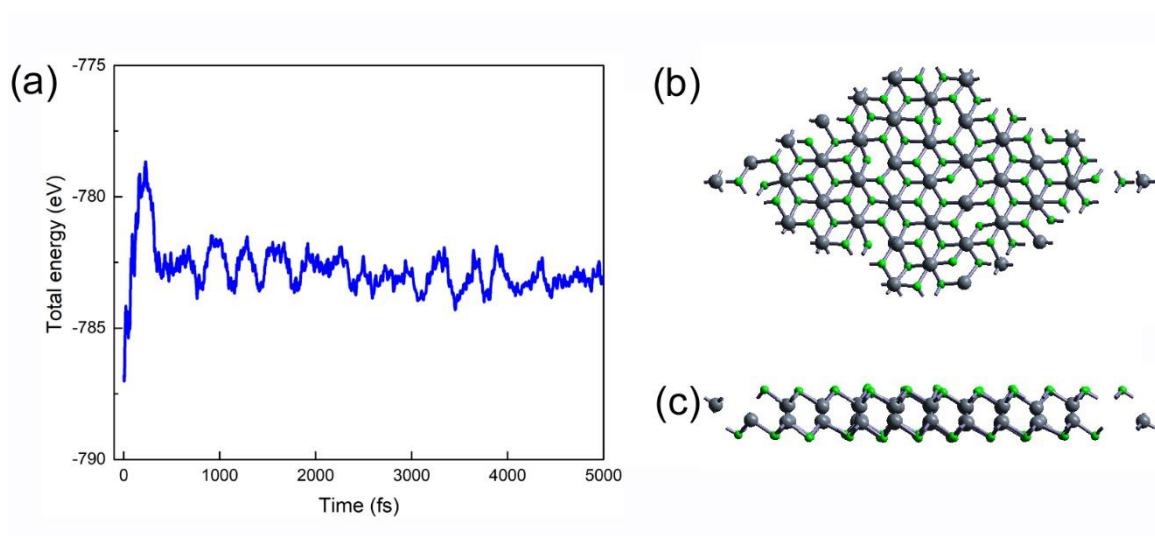


Figure S8. (a) The variation of the total energy of β -C₂Bi₂ with time in AIMD simulations at 300 K, (b) and (c) show the top view and side view of the final geometry structure, respectively.

III. Phonon dispersions

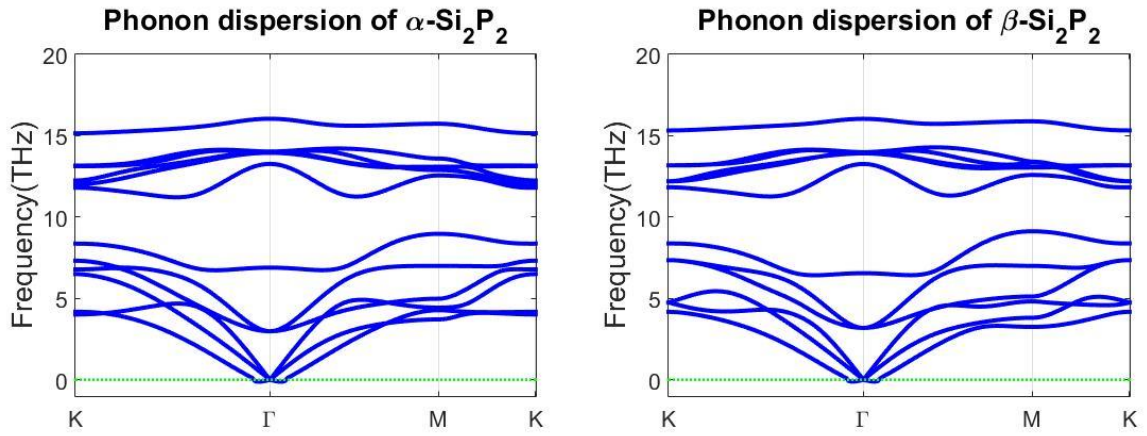


Figure S9

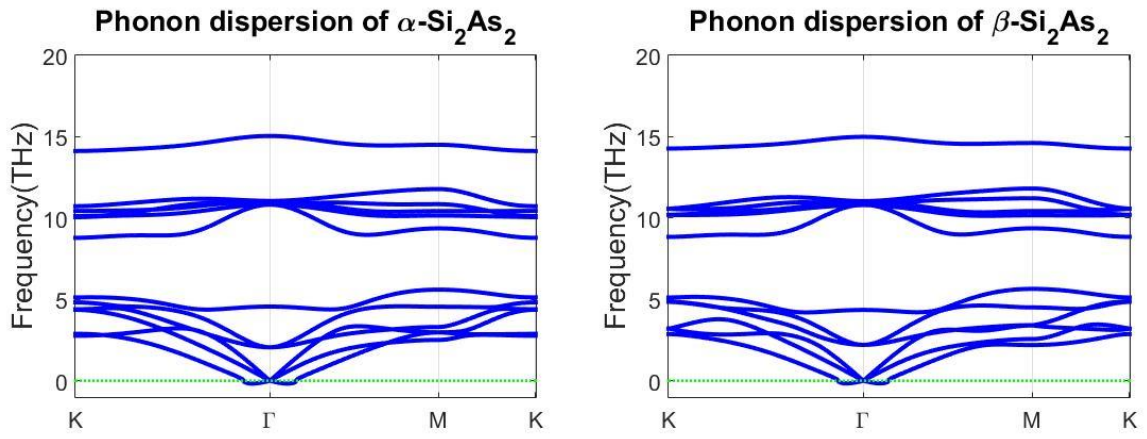


Figure S10

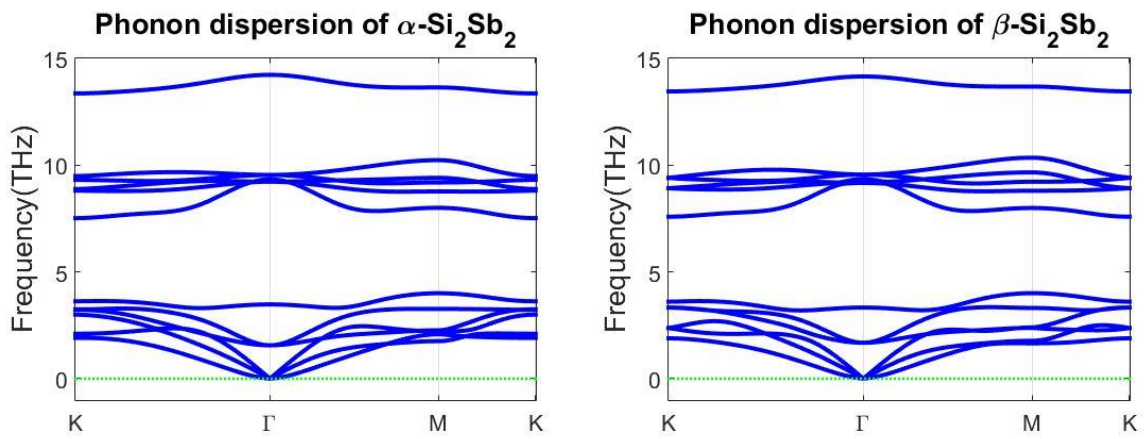


Figure S11

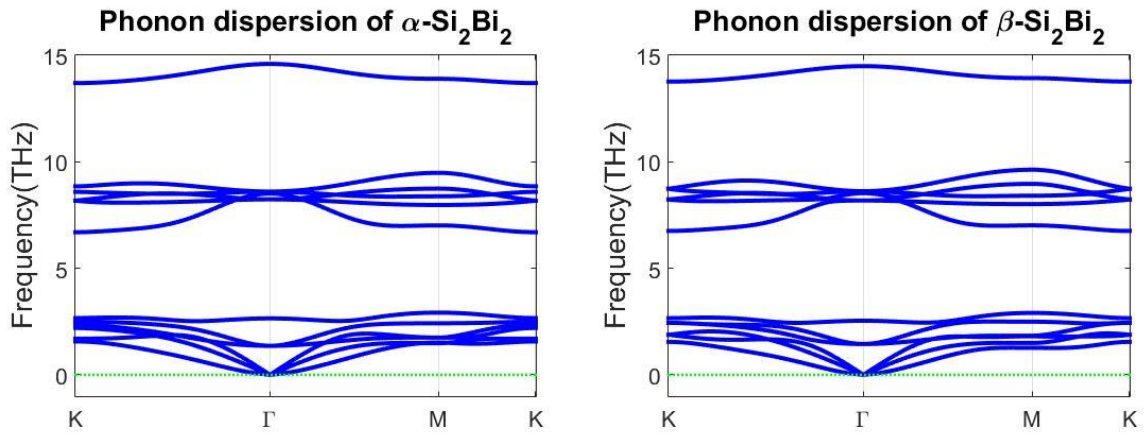


Figure S12

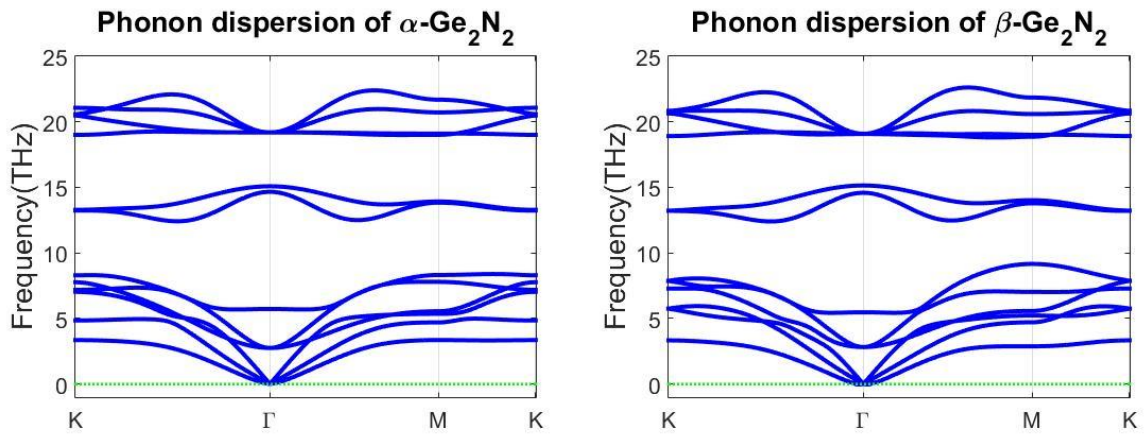


Figure S13

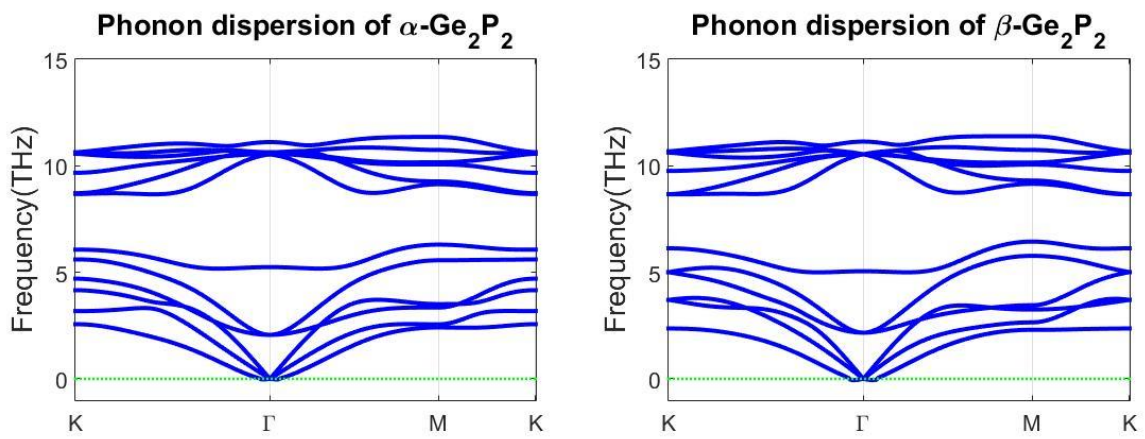


Figure S14

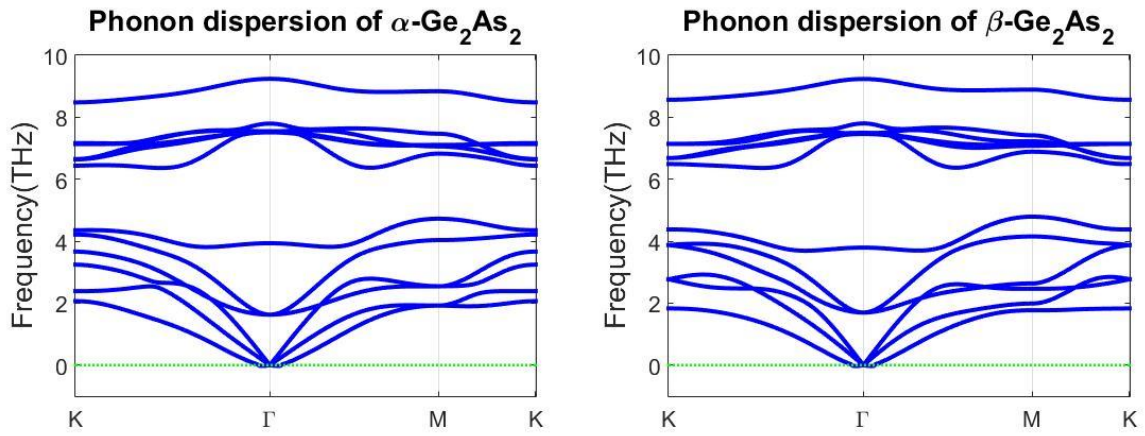


Figure S15

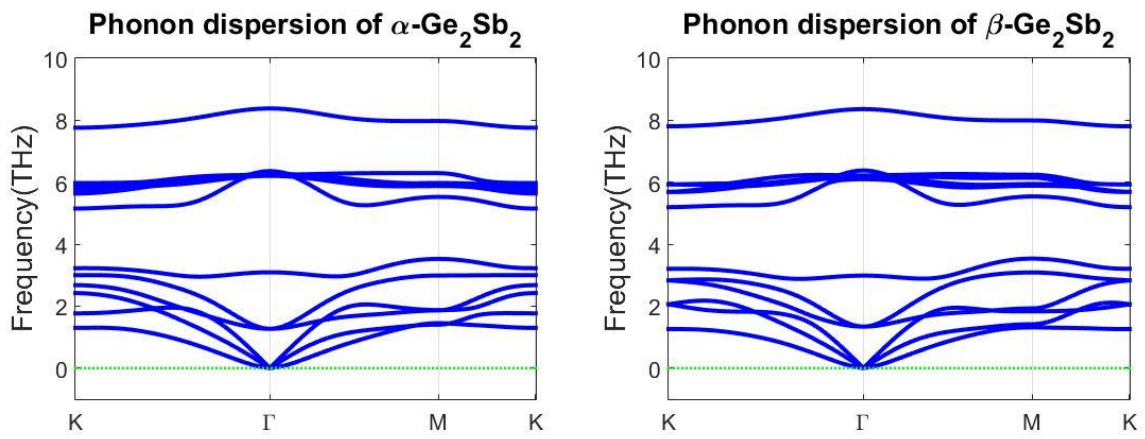


Figure S16

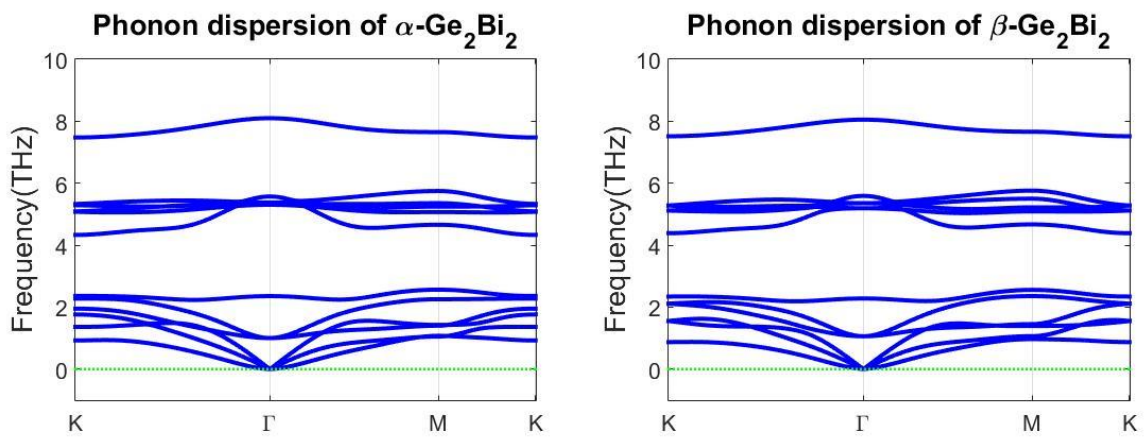


Figure S17

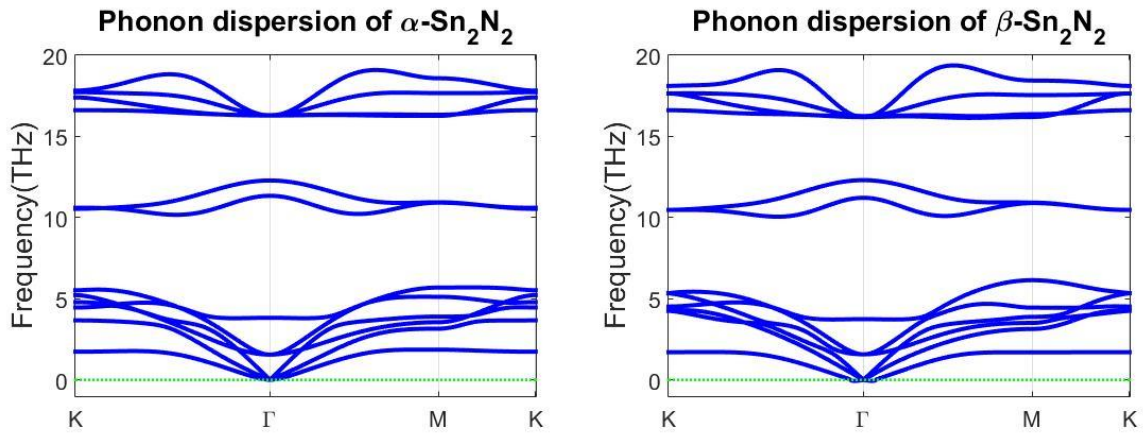


Figure S18

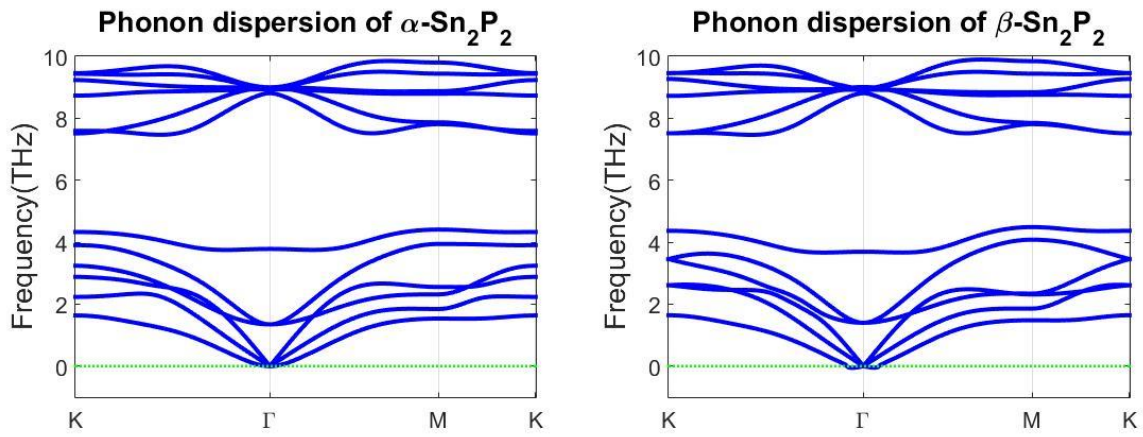


Figure S19

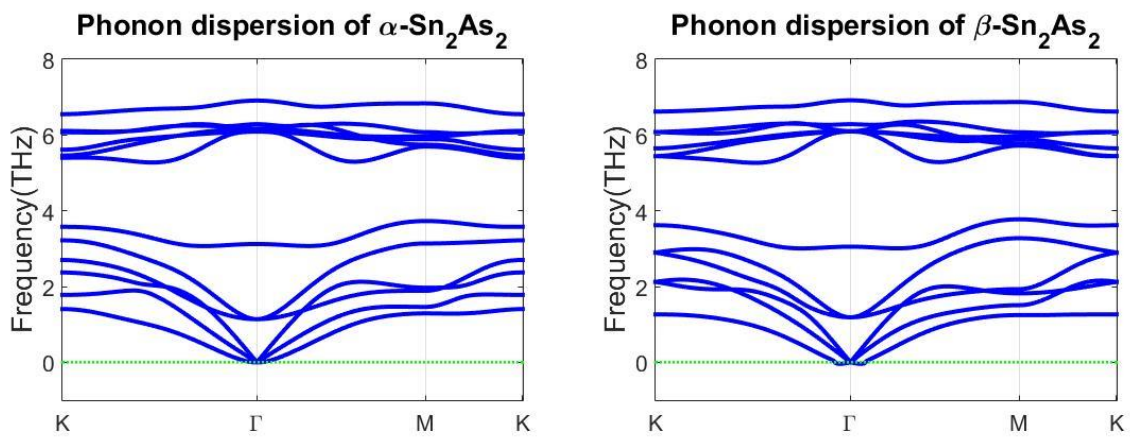


Figure S20

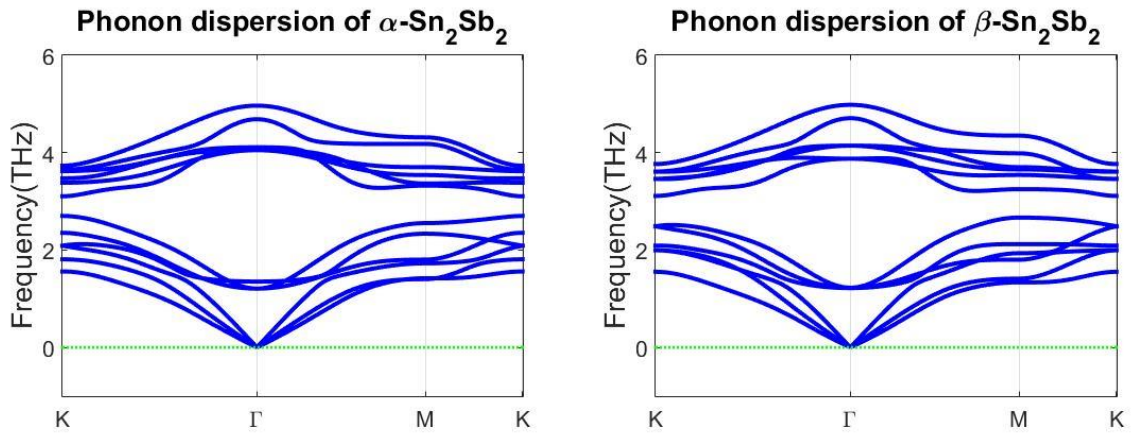


Figure S21

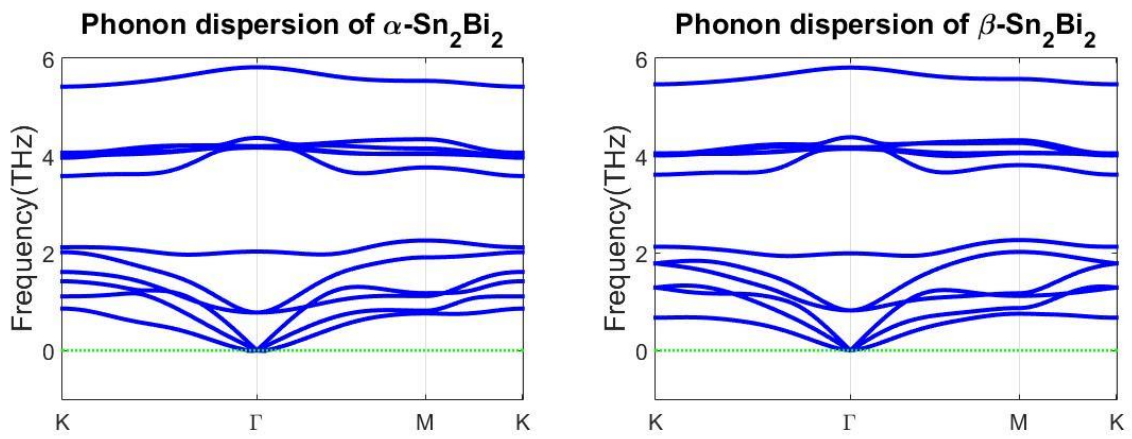


Figure S22

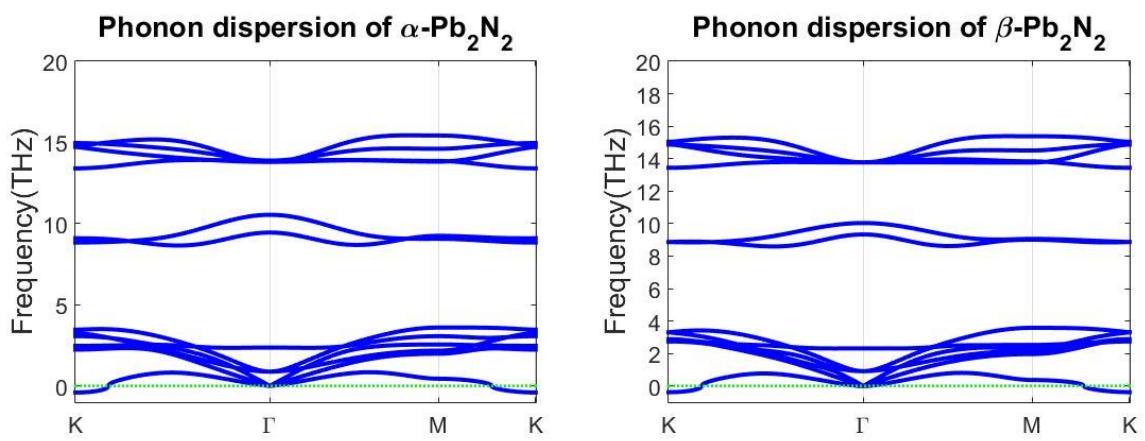


Figure S23

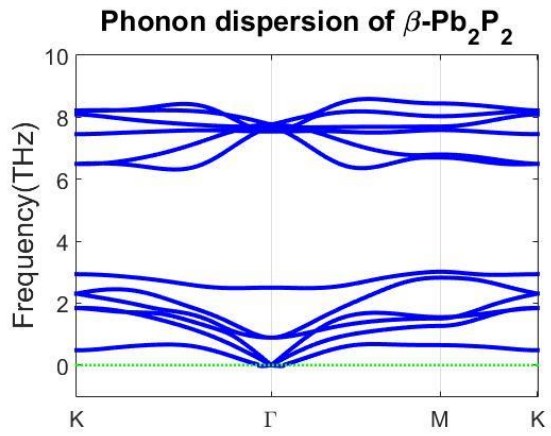
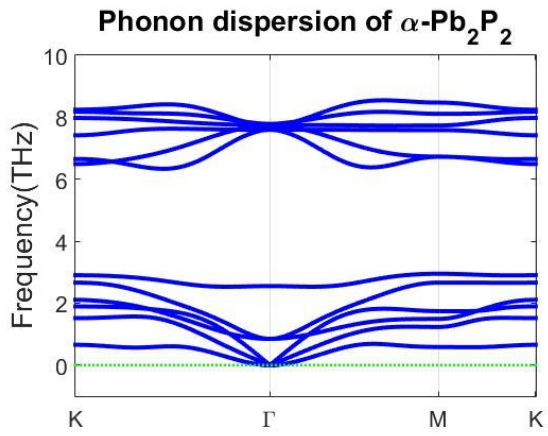


Figure S24

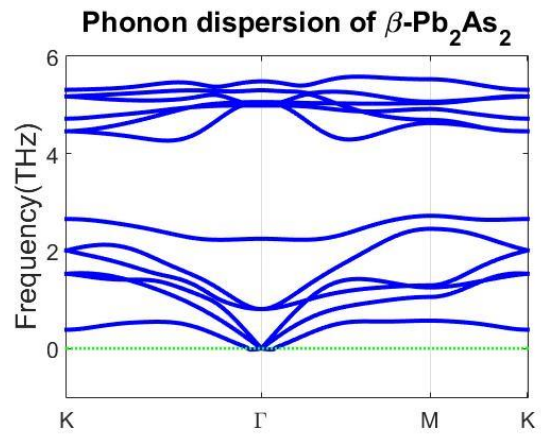
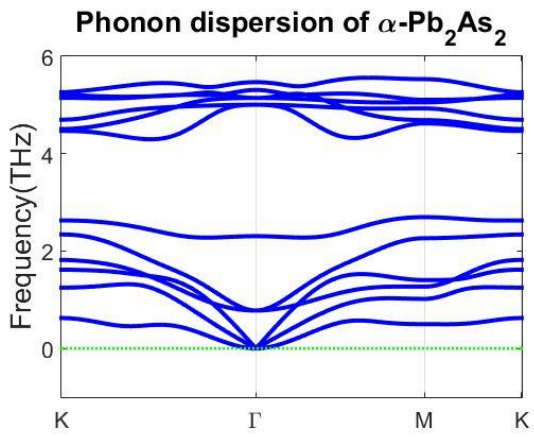


Figure S25

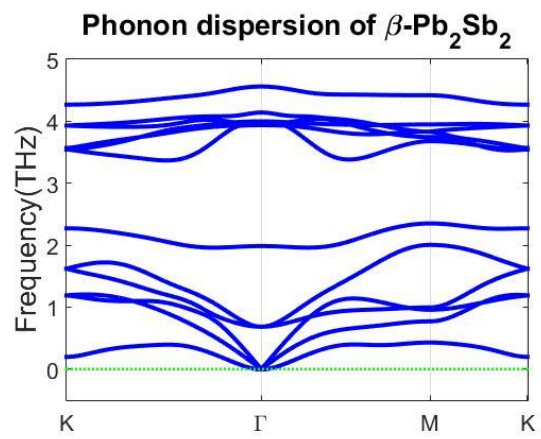
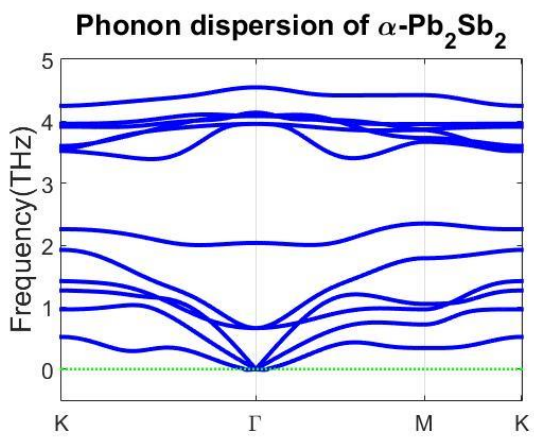


Figure S26

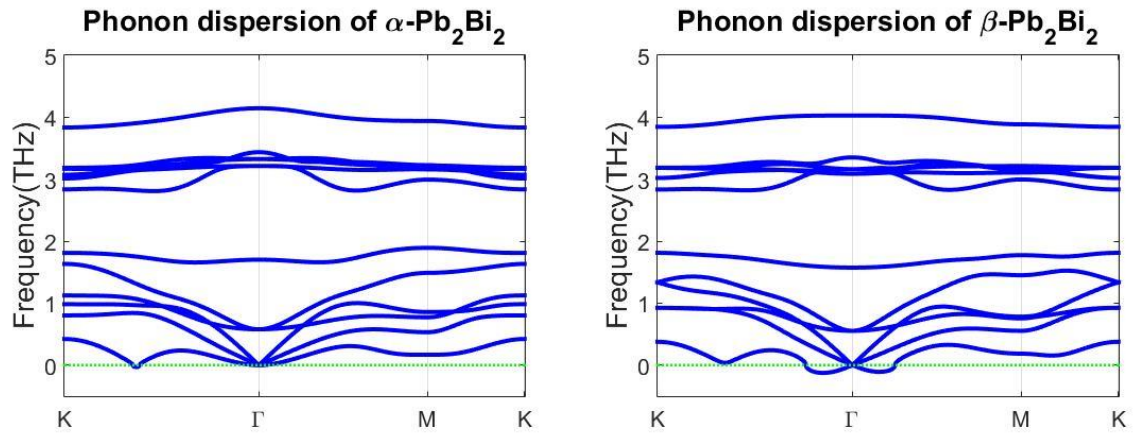


Figure S27

IV. Electronic bands

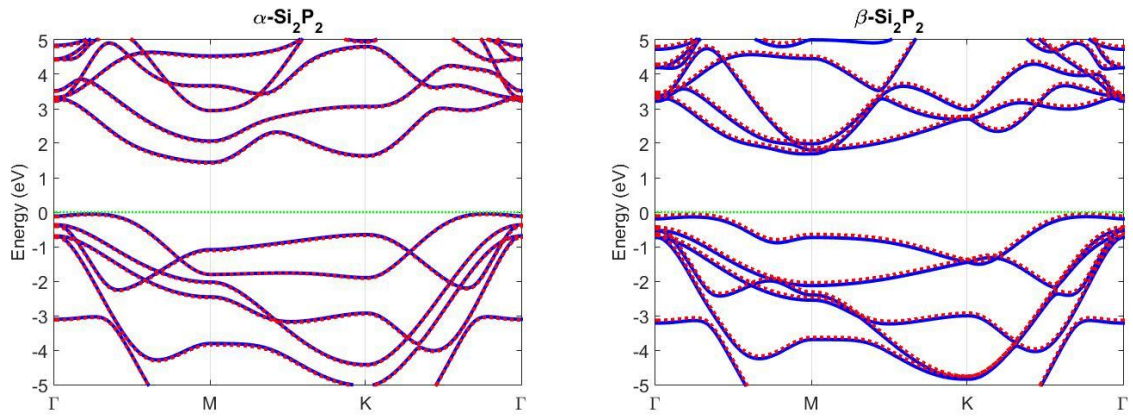


Figure S28. Electronic band of α - Si_2P_2 (left) and β - Si_2P_2 (right), the solid blue line represents the results calculated by PBE, the red dot line represents the results calculated by PBE+SOC.

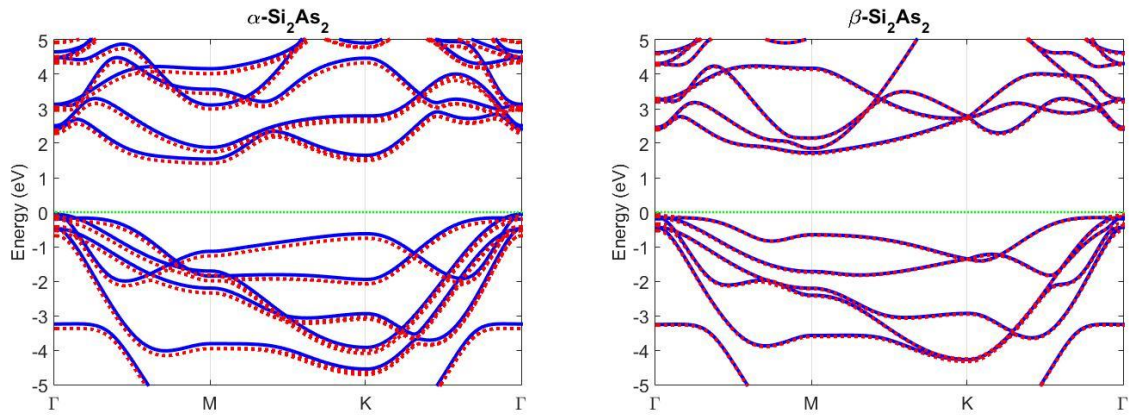


Figure S29. Electronic band of α - Si_2As_2 (left) and β - Si_2As_2 (right), the solid blue line represents the results calculated by PBE, the red dot line represents the results calculated by PBE+SOC.

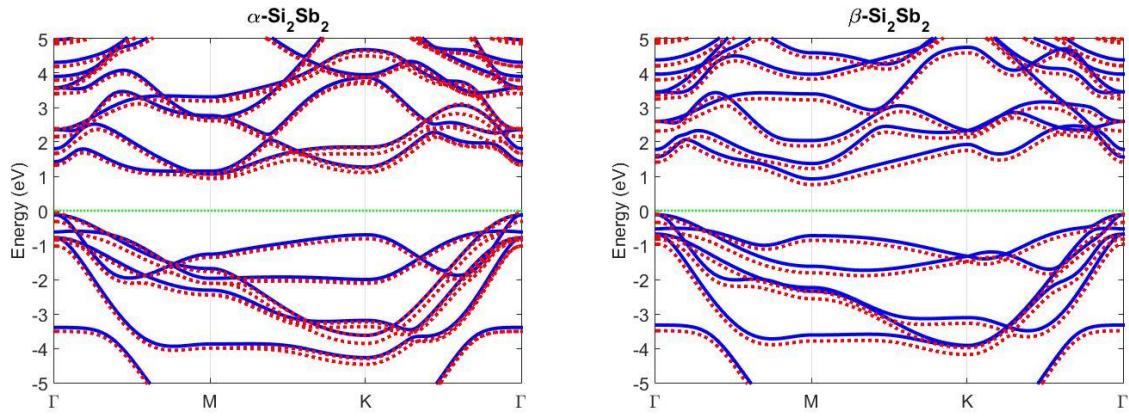


Figure S30. Electronic band of α - Si_2Sb_2 (left) and β - Si_2Sb_2 (right), the solid blue line represents the results calculated by PBE, the red dot line represents the results calculated by PBE+SOC.

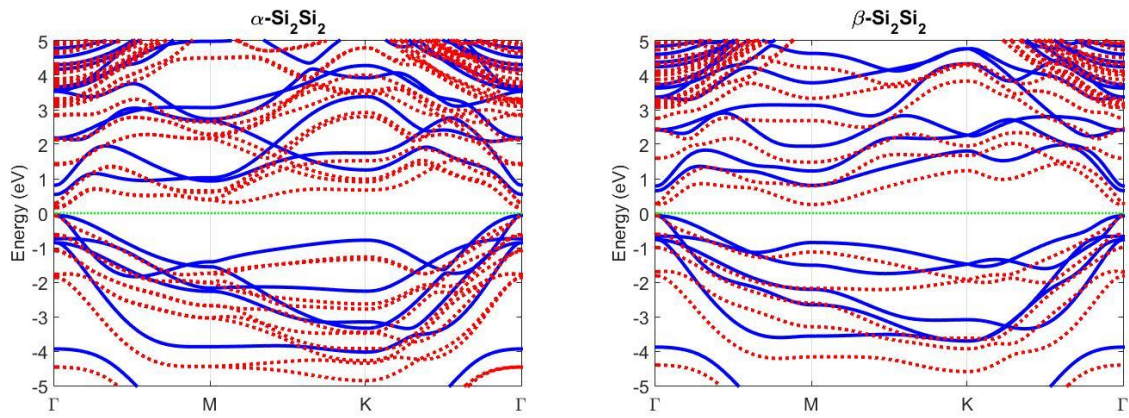


Figure S31. Electronic band of α - Si_2Bi_2 (left) and β - Si_2Bi_2 (right), the solid blue line represents the results calculated by PBE, the red dot line represents the results calculated by PBE+SOC.

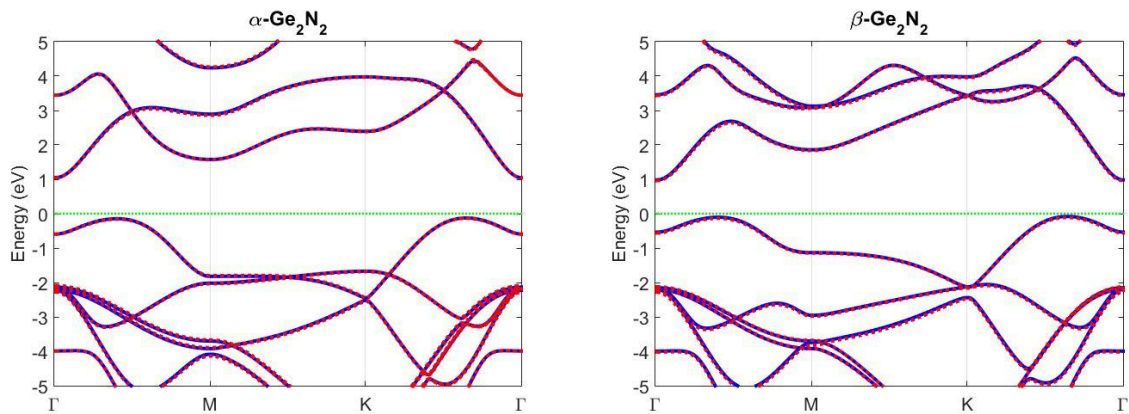


Figure S32. Electronic band of α - Ge_2N_2 (left) and β - Ge_2N_2 (right), the solid blue line represents the results calculated by PBE, the red dot line represents the results calculated by PBE+SOC.

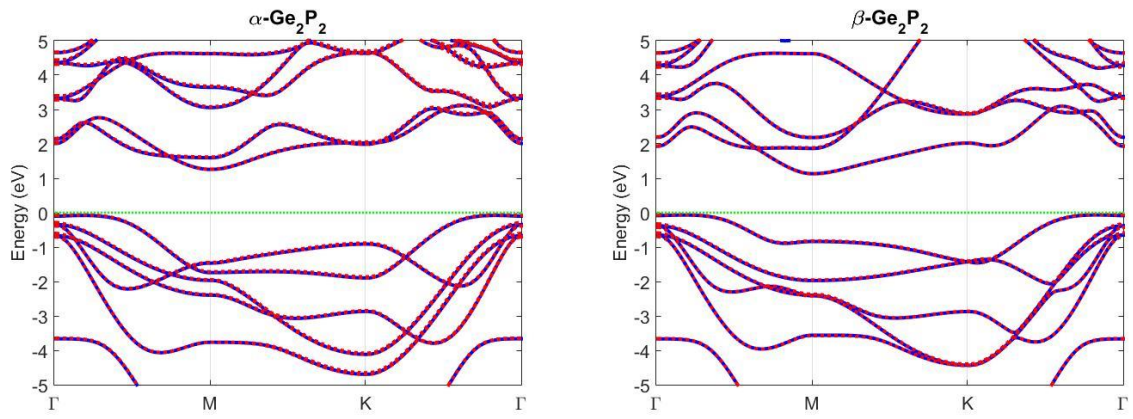


Figure S33. Electronic band of α -Ge₂P₂ (left) and β -Ge₂P₂ (right), the solid blue line represents the results calculated by PBE, the red dot line represents the results calculated by PBE+SOC.

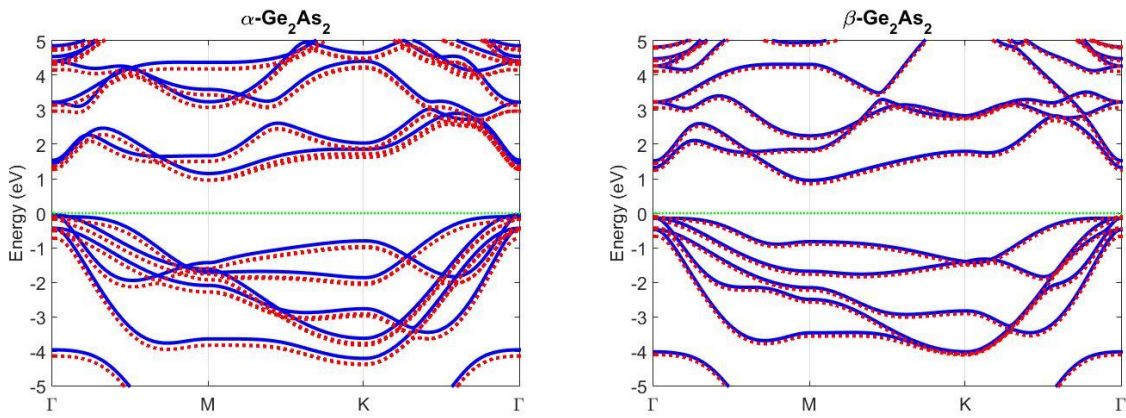


Figure S34. Electronic band of α -Ge₂As₂ (left) and β -Ge₂As₂ (right), the solid blue line represents the results calculated by PBE, the red dot line represents the results calculated by PBE+SOC.

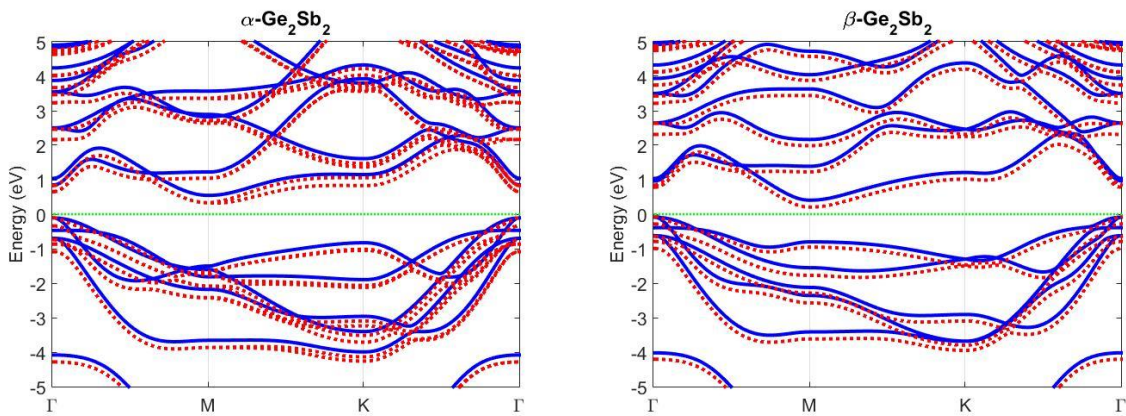


Figure S35. Electronic band of α -Ge₂Sb₂ (left) and β -Ge₂Sb₂ (right), the solid blue line represents the results calculated by PBE, the red dot line represents the results calculated by PBE+SOC.

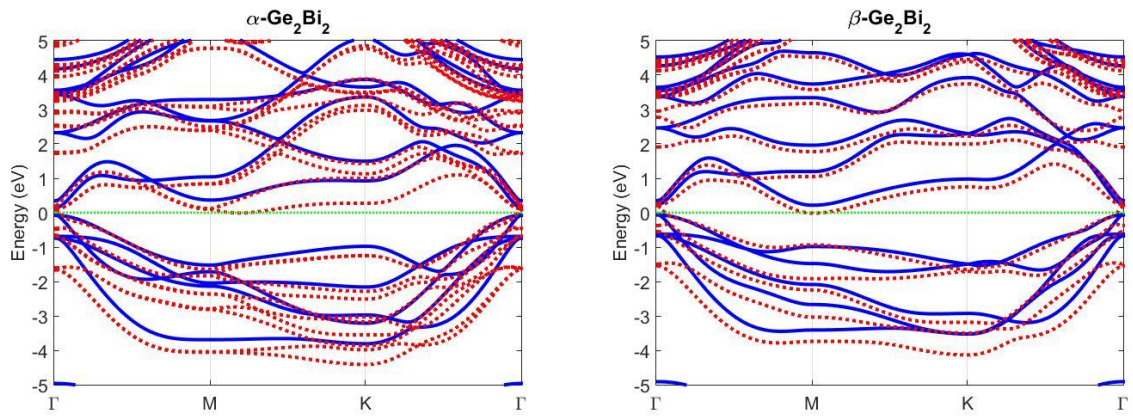


Figure S36. Electronic band of α -Ge₂Bi₂ (left) and β -Ge₂Bi₂ (right), the solid blue line represents the results calculated by PBE, the red dot line represents the results calculated by PBE+SOC.

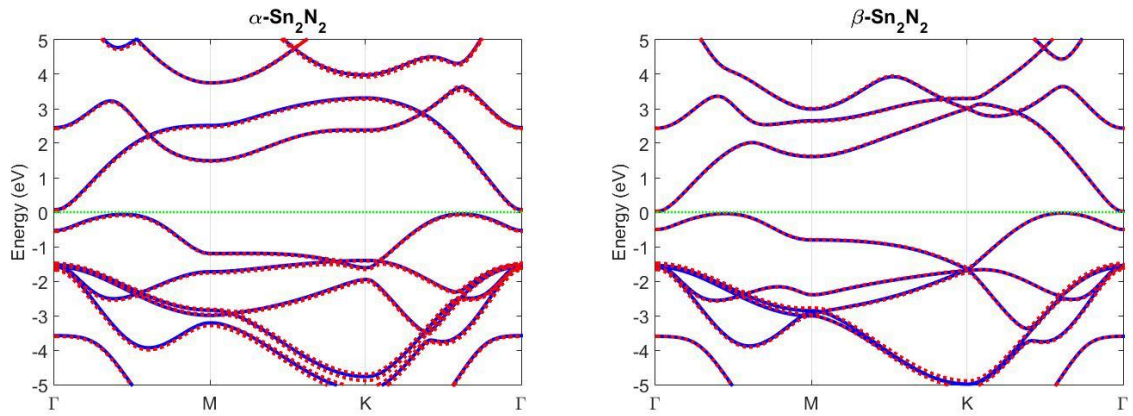


Figure S37. Electronic band of α -Sn₂N₂ (left) and β -Sn₂N₂ (right), the solid blue line represents the results calculated by PBE, the red dot line represents the results calculated by PBE+SOC.

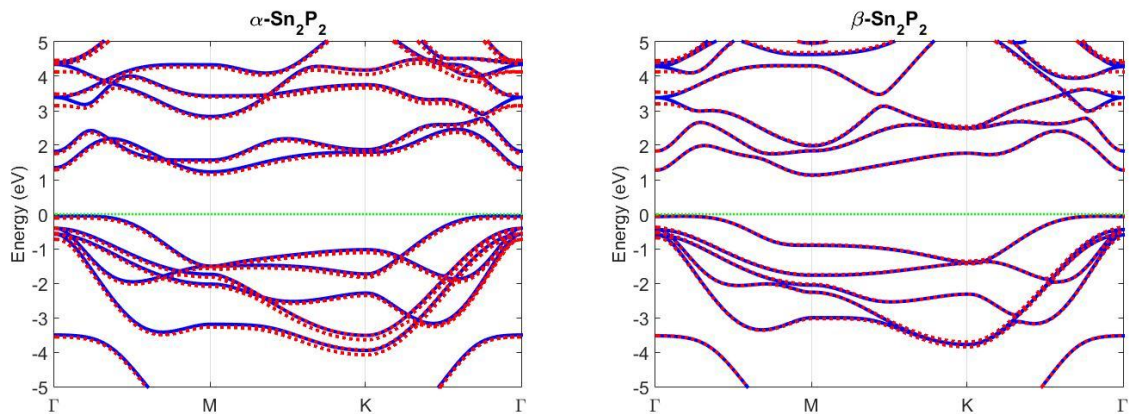


Figure S38. Electronic band of α -Sn₂P₂ (left) and β -Sn₂P₂ (right), the solid blue line represents the results calculated by PBE, the red dot line represents the results calculated by PBE+SOC.

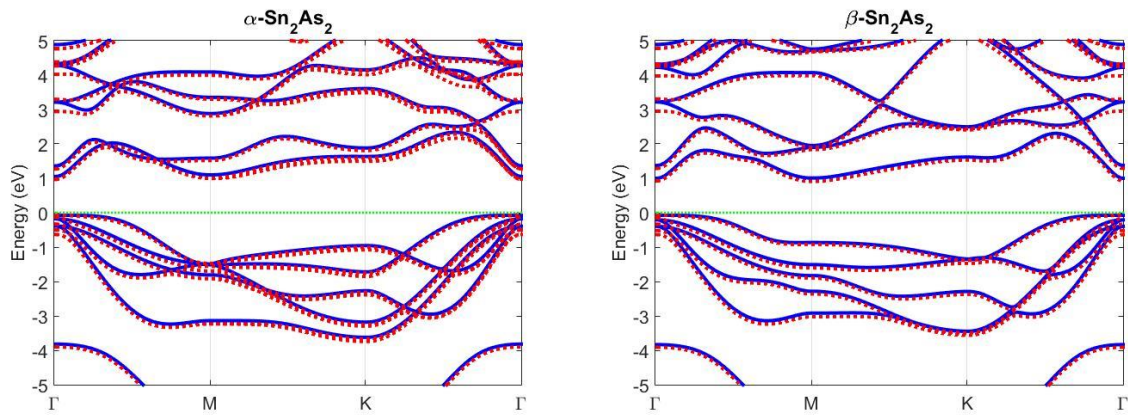


Figure S39. Electronic band of α - Sn_2As_2 (left) and β - Sn_2As_2 (right), the solid blue line represents the results calculated by PBE, the red dot line represents the results calculated by PBE+SOC.

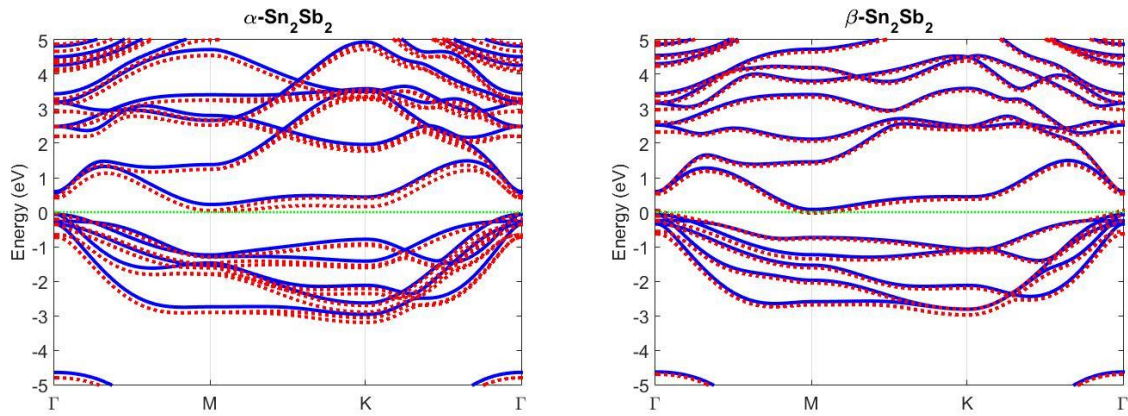


Figure S40. Electronic band of α - Sn_2Sb_2 (left) and β - Sn_2Sb_2 (right), the solid blue line represents the results calculated by PBE, the red dot line represents the results calculated by PBE+SOC.

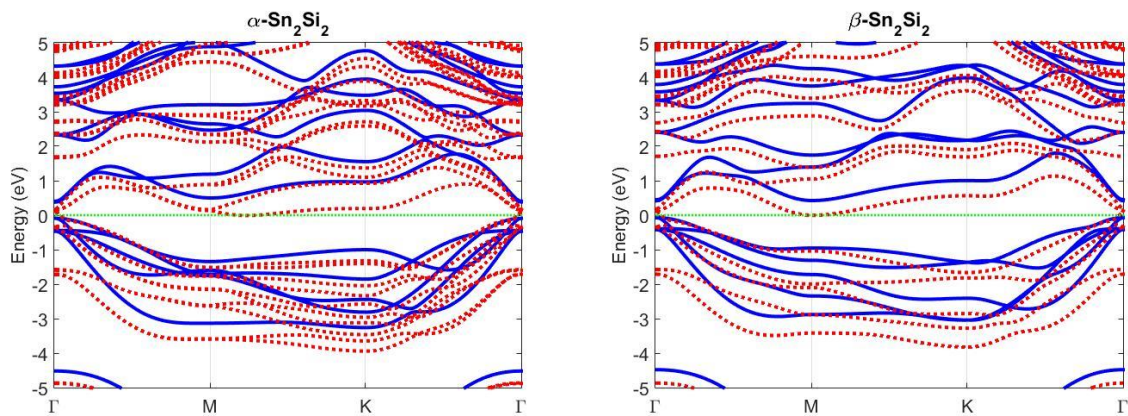


Figure S41. Electronic band of α - Sn_2Bi_2 (left) and β - Sn_2Bi_2 (right), the solid blue line represents the results calculated by PBE, the red dot line represents the results calculated by PBE+SOC.

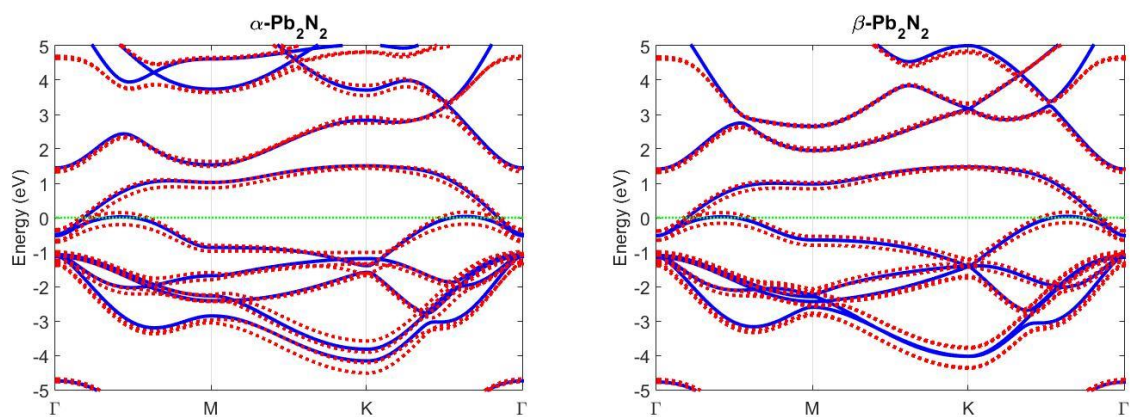


Figure S42. Electronic band of α - Pb_2N_2 (left) and β - Pb_2N_2 (right), the solid blue line represents the results calculated by PBE, the red dot line represents the results calculated by PBE+SOC.

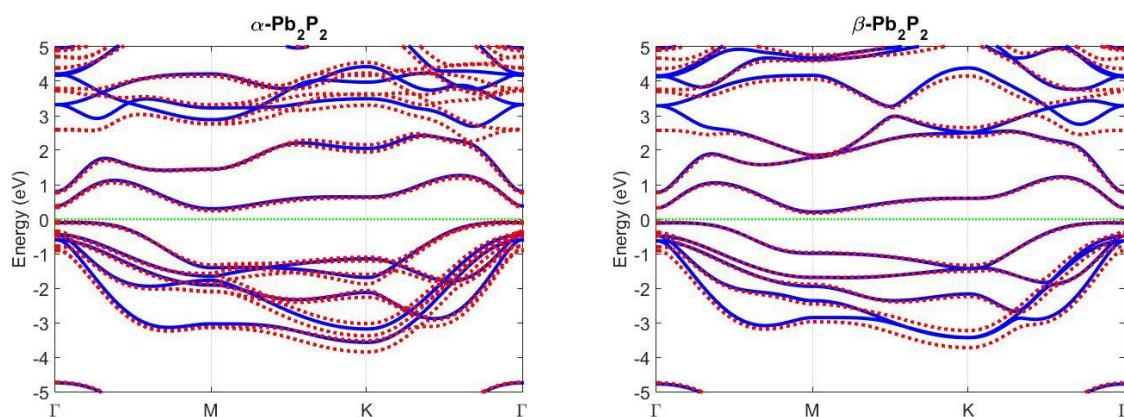


Figure S43. Electronic band of α - Pb_2P_2 (left) and β - Pb_2P_2 (right), the solid blue line represents the results calculated by PBE, the red dot line represents the results calculated by PBE+SOC.

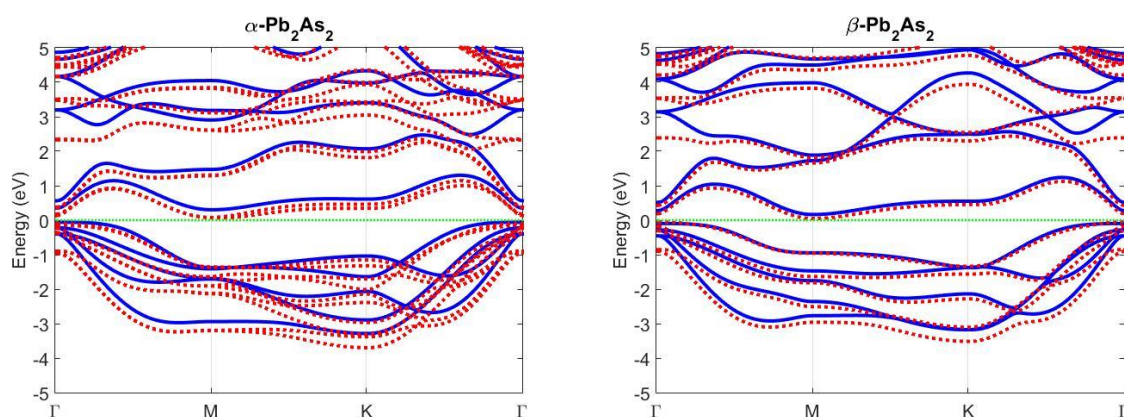


Figure S44. Electronic band of α - Pb_2As_2 (left) and β - Pb_2As_2 (right), the solid blue line represents the results calculated by PBE, the red dot line represents the results calculated by PBE+SOC.

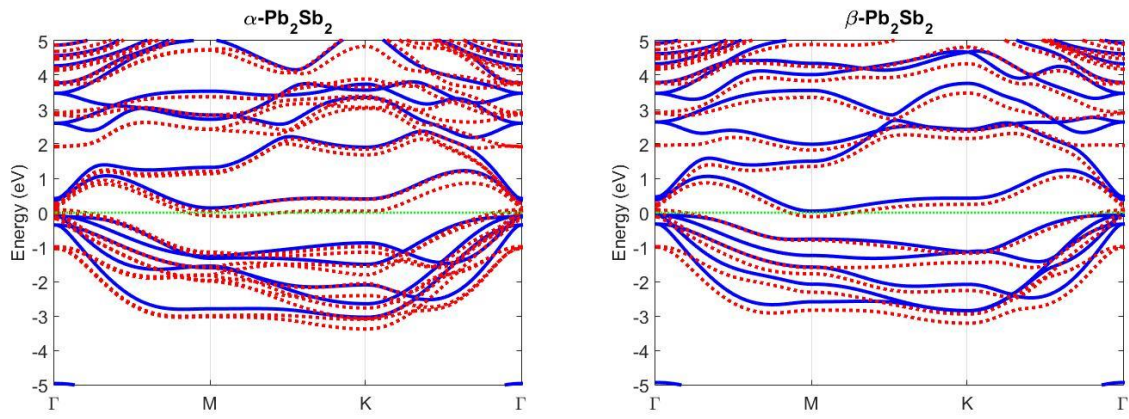


Figure S45. Electronic band of α -Pb₂Sb₂ (left) and β -Pb₂Sb₂ (right), the solid blue line represents the results calculated by PBE, the red dot line represents the results calculated by PBE+SOC.

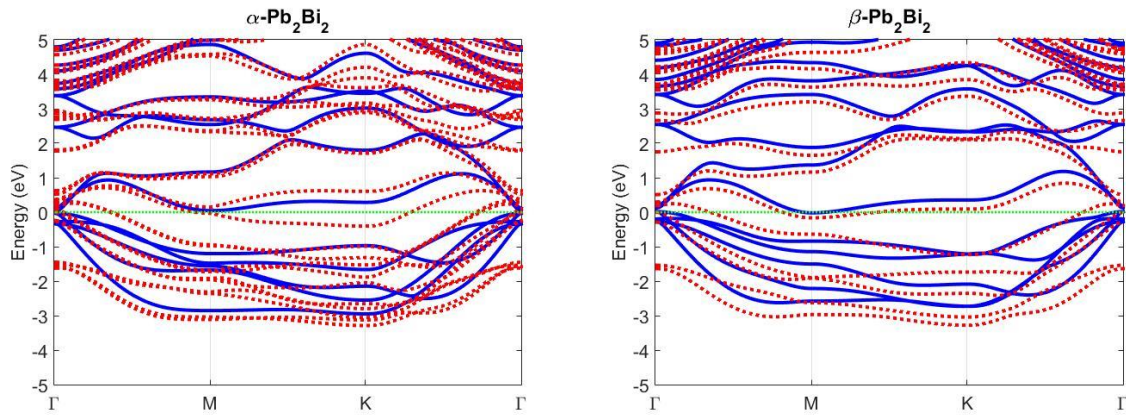


Figure S46. Electronic band of α -Pb₂Bi₂ (left) and β -Pb₂Bi₂ (right), the solid blue line represents the results calculated by PBE, the red dot line represents the results calculated by PBE+SOC.

V. Dependence of energy gap on the strain

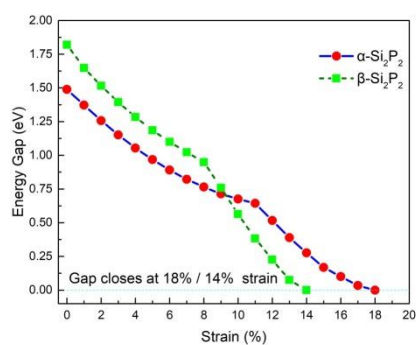


Figure S47. Dependence of energy gap on the strain of α -Si₂P₂ and β -Si₂P₂.

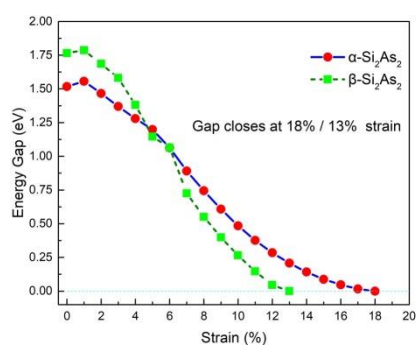


Figure S48. Dependence of energy gap on the strain of α -Si₂As₂ and β -Si₂As₂.

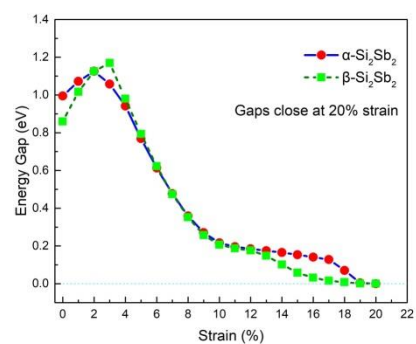


Figure S49. Dependence of energy gap on the strain of α -Si₂Sb₂ and β -Si₂Sb₂.

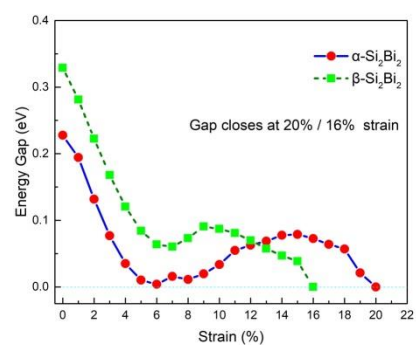


Figure S50. Dependence of energy gap on the strain of α -Si₂Bi₂ and β -Si₂Bi₂.

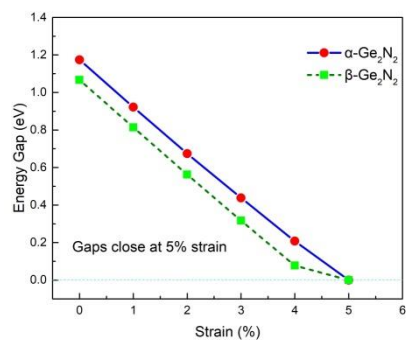


Figure S51. Dependence of energy gap on the strain of α -Ge₂N₂ and β -Ge₂N₂.

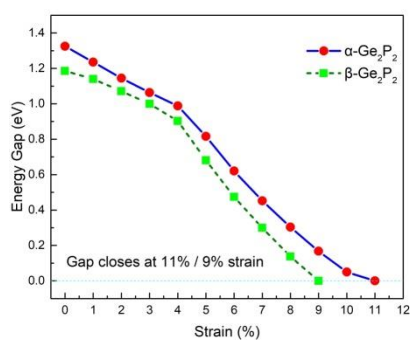


Figure S52. Dependence of energy gap on the strain of α -Ge₂P₂ and β -Ge₂P₂.

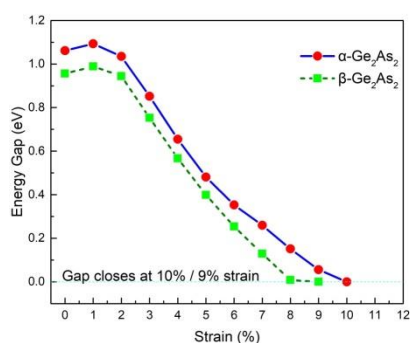


Figure S53. Dependence of energy gap on the strain of α -Ge₂As₂ and β -Ge₂As₂.

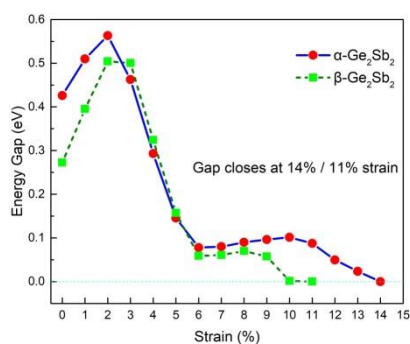


Figure S54. Dependence of energy gap on the strain of α -Ge₂Sb₂ and β -Ge₂Sb₂.

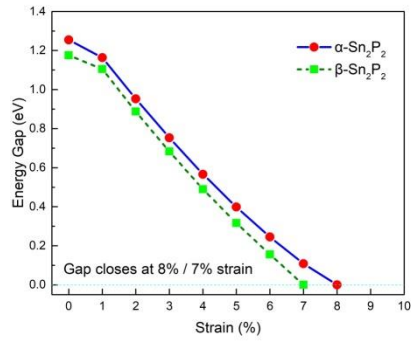


Figure S55. Dependence of energy gap on the strain of α -Sn₂P₂ and β -Sn₂P₂.

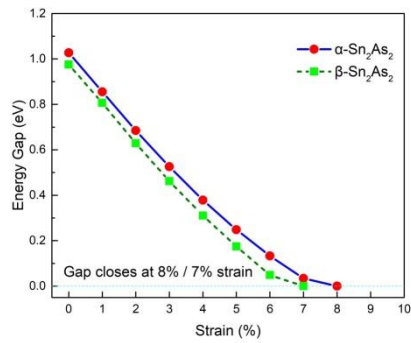


Figure S56. Dependence of energy gap on the strain of α -Sn₂As₂ and β -Sn₂As₂.

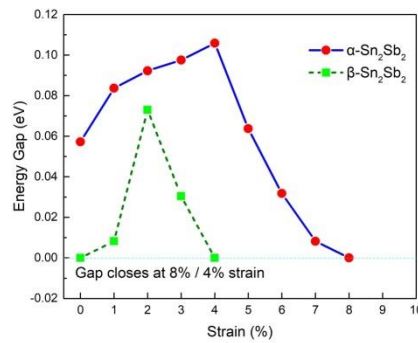


Figure S57. Dependence of energy gap on the strain of α -Sn₂Sb₂ and β -Sn₂Sb₂.

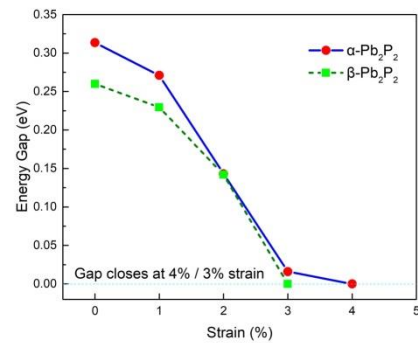


Figure S58. Dependence of energy gap on the strain of α -Pb₂P₂ and β -Pb₂P₂.

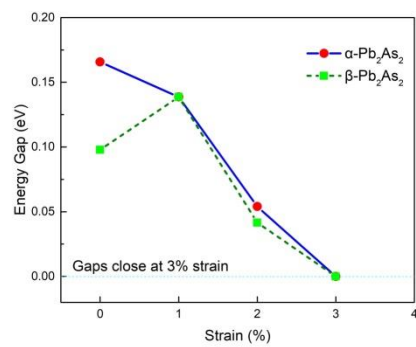


Figure S59. Dependence of energy gap on the strain of α - Pb_2As_2 and β - Pb_2As_2 .

VI. Electronic band parameters

Table S5. Electronic band parameters of Si_2Y_2 (Y=N, P, As, Sb, and Bi) in the PBE background.

Phase	PBE			PBE+SOC			Δ	ε_C (%)
	Gap1 (eV)	CBM position	VBM position	Gap2 (eV)	CBM position	VBM position		
α - Si_2N_2 [1]	1.73 ^{<i>i</i>}	M	K- Γ	/	/	/	/	17 ^a
β - Si_2N_2 [1]	1.89 ^{<i>i</i>}	M	K- Γ	/	/	/	/	16 ^a
α - Si_2P_2	1.489 ^{<i>i</i>}	M	Γ -K	1.486 ^{<i>i</i>}	M	Γ -K	-0.003	18 ^b
β - Si_2P_2	1.820 ^{<i>i</i>}	M	Γ -K	1.822 ^{<i>i</i>}	M	Γ -K	0.002	14 ^b
α - Si_2As_2	1.60 ^{<i>i</i>}	M	Γ	1.52 ^{<i>i</i>}	M	Γ	-0.08	18 ^b
β - Si_2As_2	1.86 ^{<i>i</i>}	M	Γ	1.77 ^{<i>i</i>}	M	Γ	-0.09	13 ^b
α - Si_2Sb_2	1.19 ^{<i>i</i>}	M	Γ	0.99 ^{<i>i</i>}	M	Γ	-0.2	20 ^b
β - Si_2Sb_2	1.04 ^{<i>i</i>}	M	Γ	0.86 ^{<i>i</i>}	M	Γ	-0.18	20 ^b
α - Si_2Bi_2	0.61 ^{<i>d</i>}	Γ	Γ	0.23 ^{<i>d</i>}	Γ	Γ	-0.38	20 ^b
β - Si_2Bi_2	0.73 ^{<i>d</i>}	Γ	Γ	0.33 ^{<i>i</i>}	M	Γ	0.4	16 ^b

The superscript *i* represents the direct gap, and *d* represents the indirect gap. Gap1 and Gap2 represent the band gaps calculated by PBE and PBE+SOC, respectively, $\Delta = \text{Gap2} - \text{Gap1}$. ε_C denotes the critical strain from insulativity to metallicity.

^a Represents the critical stain in the PBE background.

^b Represents the critical stain in the PBE+SOC background.

Table S6. Electronic band parameters of Ge₂Y₂(Y=N, P, As, Sb, and Bi) in the PBE background.

Phase	PBE			PBE+SOC			Δ	ϵ_C (%)
	Gap1 (eV)	CBM position	VBM position	Gap2 (eV)	CBM position	VBM position		
α -Ge ₂ N ₂	1.172 ^{<i>i</i>}	Γ	Γ -K	1.174 ^{<i>i</i>}	Γ	Γ -K	0.002	5 ^b
β -Ge ₂ N ₂	1.062 ^{<i>i</i>}	Γ	Γ -K	1.067 ^{<i>i</i>}	Γ	Γ -K	0.005	5 ^b
α -Ge ₂ P ₂	1.34 ^{<i>i</i>}	M	Γ -K	1.32 ^{<i>i</i>}	M	Γ -K	-0.02	11 ^b
β -Ge ₂ P ₂	1.201 ^{<i>i</i>}	M	Γ -K	1.185 ^{<i>i</i>}	M	Γ -K	-0.016	9 ^b
α -Ge ₂ As ₂	1.195 ^{<i>i</i>}	M	Γ	1.062 ^{<i>i</i>}	M	Γ	-0.133	10 ^b
β -Ge ₂ As ₂	1.091 ^{<i>i</i>}	M	Γ	0.956 ^{<i>i</i>}	M	Γ	-0.135	9 ^b
α -Ge ₂ Sb ₂	0.656 ^{<i>i</i>}	M	Γ	0.426 ^{<i>i</i>}	M	Γ	-0.23	14 ^b
β -Ge ₂ Sb ₂	0.495 ^{<i>i</i>}	M	Γ	0.273 ^{<i>i</i>}	M	Γ	-0.222	11 ^b
α -Ge ₂ Bi ₂	0.224 ^{<i>d</i>}	Γ	Γ	0	/	/	-0.224	/
β -Ge ₂ Bi ₂	0.284 ^{<i>i</i>}	M	Γ	0	/	/	-0.284	/

The superscript *i* represents the direct gap, and *d* represents the indirect gap. Gap1 and Gap2 represent the band gaps calculated by PBE and PBE+SOC, respectively, Δ =Gap2-Gap1. ϵ_C denotes the critical strain from insulativity to metallicity.

^b Represents the critical stain in the PBE+SOC background.

Table S7. Electronic band parameters of Sn₂Y₂(Y=N, P, As, Sb, and Bi) in the PBE background.

Phase	PBE			PBE+SOC			Δ	ϵ_C (%)
	Gap1 (eV)	CBM position	VBM position	Gap2 (eV)	CBM position	VBM position		
α -Sn ₂ N ₂	0.125 ^{<i>i</i>}	Γ	Γ -K	0.123 ^{<i>i</i>}	Γ	Γ -K	-0.002	1 ^b
β -Sn ₂ N ₂	0.050 ^{<i>i</i>}	Γ	Γ -K	0.058 ^{<i>i</i>}	Γ	Γ -K	0.008	1 ^b
α -Sn ₂ P ₂	1.280 ^{<i>i</i>}	M	Γ -K	1.255 ^{<i>i</i>}	M	Γ -K	-0.025	8 ^b
β -Sn ₂ P ₂	1.196 ^{<i>i</i>}	M	Γ -K	1.175 ^{<i>i</i>}	M	Γ -K	-0.021	7 ^b
α -Sn ₂ As ₂	1.128 ^{<i>d</i>}	Γ	Γ	1.027 ^{<i>d</i>}	Γ	Γ	-0.101	8 ^b
β -Sn ₂ As ₂	1.075 ^{<i>d</i>}	Γ	Γ	0.975 ^{<i>i</i>}	Γ	Γ	-0.1	7 ^b
α -Sn ₂ Sb ₂	0.289 ^{<i>i</i>}	M	Γ	0.057 ^{<i>i</i>}	M-K	Γ	-0.232	8 ^b
β -Sn ₂ Sb ₂	0.151 ^{<i>i</i>}	M	Γ	0	/	/	-0.151	4 ^b
α -Sn ₂ Bi ₂	0.475 ^{<i>d</i>}	Γ	Γ	0	/	/	-0.475	/
β -Sn ₂ Bi ₂	0.493 ^{<i>d</i>}	Γ	Γ	0	/	/	-0.493	/

The superscript *i* represents the direct gap, and *d* represents the indirect gap. Gap1 and Gap2 represent the band gaps calculated by PBE and PBE+SOC, respectively, Δ =Gap2-Gap1. ϵ_C denotes the critical strain from insulativity to metallicity.

^b Represents the critical stain in the PBE+SOC background.

Table S8. Electronic band parameters of Pb_2Y_2 (Y=N, P, As, Sb, and Bi) in the PBE background.

Phase	PBE			PBE+SOC			Δ	ε_C (%)
	Gap1 (eV)	CBM position	VBM position	Gap2 (eV)	CBM position	VBM position		
α - Pb_2N_2	0	/	/	0	/	/	0	/
β - Pb_2N_2	0	/	/	0	/	/	0	/
α - Pb_2P_2	0.400 ^{<i>i</i>}	M	Γ -M	0.313 ^{<i>i</i>}	M	Γ	-0.087	4 ^b
β - Pb_2P_2	0.315 ^{<i>i</i>}	M	Γ -M	0.260 ^{<i>i</i>}	M	Γ	-0.055	3 ^b
α - Pb_2As_2	0.363 ^{<i>i</i>}	M	Γ -M	0.166 ^{<i>i</i>}	M	Γ	-0.197	3 ^b
β - Pb_2As_2	0.261 ^{<i>i</i>}	M	Γ	0.098 ^{<i>i</i>}	M	Γ	-0.163	3 ^b
α - Pb_2Sb_2	0.23 ^{<i>i</i>}	M	Γ	0	/	/	-0.23	/
β - Pb_2Sb_2	0.120 ^{<i>i</i>}	M	Γ	0	/	/	-0.12	/
α - Pb_2Bi_2	0.064 ^{<i>d</i>}	Γ	Γ	0	/	/	-0.064	/
β - Pb_2Bi_2	0	/	/	0	/	/	0	/

The superscript *i* represents the direct gap, and *d* represents the indirect gap. Gap1 and Gap2 represent the band gaps calculated by PBE and PBE+SOC, respectively, $\Delta = \text{Gap2} - \text{Gap1}$. ε_C denotes the critical strain from insulativity to metallicity.

^b Represents the critical stain in the PBE+SOC background.

VII. Computational details

In the calculation of the force constants for phonon dispersions, the cut-off energy and the size of supercells are shown in Table S9.

Table S9. The cut-off energy and the size of the supercells

phase	cut-off energy (eV)	size of the supercell	phase	cut-off energy (eV)	size of the supercell	phase	cut-off energy (eV)	size of the supercell
α -C ₂ P ₂	520	6×6×1	α -Si ₂ Bi ₂	350	4×4×1	α -Sn ₂ As ₂	280	4×4×1
β -C ₂ P ₂	520	6×6×1	β -Si ₂ Bi ₂	350	4×4×1	β -Sn ₂ As ₂	280	5×5×1
α -C ₂ As ₂	520	5×5×1	α -Ge ₂ N ₂	520	4×4×1	α -Sn ₂ Sb ₂	230	4×4×1
β -C ₂ As ₂	520	5×5×1	β -Ge ₂ N ₂	520	4×4×1	β -Sn ₂ Sb ₂	230	4×4×1
α -C ₂ Sb ₂	520	6×6×1	α -Ge ₂ P ₂	335	4×4×1	α -Sn ₂ Bi ₂	600	4×4×1
β -C ₂ Sb ₂	520	6×6×1	β -Ge ₂ P ₂	335	5×5×1	β -Sn ₂ Bi ₂	600	5×5×1
α -C ₂ Bi ₂	600	5×5×1	α -Ge ₂ As ₂	280	4×4×1	α -Pb ₂ N ₂	520	4×4×1
β -C ₂ Bi ₂	600	5×5×1	β -Ge ₂ As ₂	280	5×5×1	β -Pb ₂ N ₂	520	5×5×1
α -Si ₂ N ₂	450	4×4×1	α -Ge ₂ Sb ₂	230	5×5×1	α -Pb ₂ P ₂	335	4×4×1
β -Si ₂ N ₂	450	4×4×1	β -Ge ₂ Sb ₂	230	5×5×1	β -Pb ₂ P ₂	335	5×5×1
α -Si ₂ P ₂	335	5×5×1	α -Ge ₂ Bi ₂	230	5×5×1	α -Pb ₂ As ₂	280	4×4×1
β -Si ₂ P ₂	335	5×5×1	β -Ge ₂ Bi ₂	230	5×5×1	β -Pb ₂ As ₂	280	5×5×1
α -Si ₂ As ₂	320	5×5×1	α -Sn ₂ N ₂	600	4×4×1	α -Pb ₂ Sb ₂	230	4×4×1
β -Si ₂ As ₂	320	5×5×1	β -Sn ₂ N ₂	600	4×4×1	β -Pb ₂ Sb ₂	230	5×5×1
α -Si ₂ Sb ₂	320	5×5×1	α -Sn ₂ P ₂	335	4×4×1	α -Pb ₂ Bi ₂	138	4×4×1
β -Si ₂ Sb ₂	320	5×5×1	β -Sn ₂ P ₂	335	4×4×1	β -Pb ₂ Bi ₂	138	4×4×1

VIII. POSCAR files of the structures

POSCAR- α -C₂P₂

```

3.0000000000000000
 0.8366183838863850 -0.4830218491457943 0.0000000000000000
 0.8366183838863850 0.4830218491457943 0.0000000000000000
 0.0000000000000000 0.0000000000000000 10.0033028495504883
C      P
 2      2

```

Direct

```

0.0000000000000000 0.0000000000000000 0.0258774575229661
0.0000000000000000 0.0000000000000000 0.9741225424770340
0.3333333333333357 0.3333333333333357 0.0549791897473604
0.3333333333333357 0.3333333333333357 0.9450208102526397

```

POSCAR- β -C₂P₂

```

3.0000000000000000
 0.8366183838863850 -0.4830218491457943 0.0000000000000000
 0.8366183838863850 0.4830218491457943 0.0000000000000000
 0.0000000000000000 0.0000000000000000 10.0033028495504883
C      P
 2      2

```

Direct

```

0.0000000000000000 0.0000000000000000 0.0258774575229661
0.0000000000000000 0.0000000000000000 0.9741225424770340
0.3333333333333357 0.3333333333333357 0.0549791897473604
-0.3333333333333357 -0.3333333333333357 0.9450208102526397

```

POSCAR- α -C₂As₂

```

1.0000000000000000
 2.69278639882923355 -1.554680952233637775 0.0000000000000000
 2.69278639882890535 1.554680952234332775 0.0000000000000000
 0.0000000000000000 0.0000000000000000 25.6013886650011280
C      As
 2      2

```

Direct

```

0.0000000000000000 0.0000000000000000 0.0298020037990700
0.0000000000000000 0.0000000000000000 0.9701979962009158
0.3333333333333357 0.3333333333333357 0.0675231569654309
0.3333333333333357 0.3333333333333357 0.9324768429345743

```

POSCAR- β -C₂As₂

```

1.0000000000000000
 2.69278639882923355 -1.554680952233637775 0.0000000000000000
 2.69278639882890535 1.554680952234332775 0.0000000000000000
 0.0000000000000000 0.0000000000000000 25.6013886650011280
C      As
 2      2

```

Direct

0.0000000000000000	0.0000000000000000	0.0298020037990700
0.0000000000000000	0.0000000000000000	0.9701979962009158
0.3333333333333357	0.3333333333333357	0.0675231569654309
-0.3333333333333357	-0.3333333333333357	0.9324768429345743

POSCAR- α -C₂Sb₂

3.3100000000000000		
0.8910807025050776	-0.5144656834609223	0.0000000000000000
0.8910807025049883	0.5144656834609004	0.0000000000000000
0.0000000000000000	0.0000000000000000	7.9895035198626543

C Sb
2 2

Direct

0.0000000000000000	0.0000000000000000	0.0288624062787197
0.0000000000000000	0.0000000000000000	0.9711375937212808
0.3333333333333357	0.3333333333333357	0.0700540507434779
0.3333333333333357	0.3333333333333357	0.9299459492565225

POSCAR- β -C₂Sb₂

3.3100000000000000		
0.8910807025050776	-0.5144656834609223	0.0000000000000000
0.8910807025049883	0.5144656834609004	0.0000000000000000
0.0000000000000000	0.0000000000000000	7.9895035198626543

C Sb
2 2

Direct

0.0000000000000000	0.0000000000000000	0.0288624062787197
0.0000000000000000	0.0000000000000000	0.9711375937212808
0.3333333333333357	0.3333333333333357	0.0700540507434779
-0.3333333333333357	-0.3333333333333357	0.9299459492565225

POSCAR- α -C₂Bi₂

1.0000000000000000		
3.1204893349827456	-1.801615358361174475	0.0000000000000000
3.12048933498237745	1.801615358361069225	0.0000000000000000
0.0000000000000000	0.0000000000000000	25.6181855773495286

C Bi
2 2

Direct

0.0000000000000000	0.0000000000000000	0.0290691034198632
0.0000000000000000	0.0000000000000000	0.9709308965801154
0.3333333333333357	0.3333333333333357	0.0740567473954728
0.3333333333333357	0.3333333333333357	0.9259432526044563

POSCAR- β -C₂Bi₂

1.0000000000000000		
3.1204893349827456	-1.801615358361174475	0.0000000000000000
3.12048933498237745	1.801615358361069225	0.0000000000000000
0.0000000000000000	0.0000000000000000	25.6181855773495286

C Bi
 2 2
 Direct
 0.0000000000000000 0.0000000000000000 0.0290691034198632
 0.0000000000000000 0.0000000000000000 0.9709308965801154
 0.3333333333333357 0.3333333333333357 0.0740567473954728
 -0.3333333333333357 -0.3333333333333357 0.9259432526044563

POSCAR- α -Si₂P₂
 1.0000000000000000
 3.05639045190647885 -1.7646078501506146 0.0000000000000000
 3.05639045190631765 1.764607850150573075 0.0000000000000000
 0.0000000000000000 0.0000000000000000 27.1966286625978064

Si P
 2 2
 Direct
 0.0000000000000000 0.0000000000000000 0.0436560124219749
 0.0000000000000000 0.0000000000000000 0.9563439875779401
 0.3333333333333357 0.3333333333333357 0.0810013235839673
 0.3333333333333357 0.3333333333333357 0.9189986764160395

POSCAR- β -Si₂P₂
 1.0000000000000000
 3.05639045190647885 -1.7646078501506146 0.0000000000000000
 3.05639045190631765 1.764607850150573075 0.0000000000000000
 0.0000000000000000 0.0000000000000000 27.1966286625978064

Si P
 2 2
 Direct
 0.0000000000000000 0.0000000000000000 0.0436560124219749
 0.0000000000000000 0.0000000000000000 0.9563439875779401
 0.3333333333333357 0.3333333333333357 0.0810013235839673
 -0.3333333333333357 -0.3333333333333357 0.9189986764160395

POSCAR- α -Si₂As₂
 1.0000000000000000
 3.1998494810974334 -1.847433959284871425 0.0000000000000000
 3.199849481097536425 1.8474339592831952 0.0000000000000000
 0.0000000000000000 0.0000000000000000 26.9957699420950554

Si As
 2 2
 Direct
 0.0000000000000000 0.0000000000000000 0.0437716381548780
 0.0000000000000000 0.0000000000000000 0.9562283618451219
 0.3333333333333357 0.3333333333333357 0.0847602391142282
 0.3333333333333357 0.3333333333333357 0.9152397608857719

POSCAR- β -Si₂As₂
 1.0000000000000000

3.1998494810974334 -1.847433959284871425 0.0000000000000000
3.199849481097536425 1.8474339592831952 0.0000000000000000
0.0000000000000000 0.0000000000000000 26.9957699420950554

Si As
2 2

Direct

0.0000000000000000 0.0000000000000000 0.0437716381548780
0.0000000000000000 0.0000000000000000 0.9562283618451219
0.3333333333333357 0.3333333333333357 0.0847602391142282
-0.3333333333333357 -0.3333333333333357 0.9152397608857719

POSCAR- α -Si₂Sb₂

1.0000000000000000
3.477529132536688375 -2.007752380784829875 0.0000000000000000
3.47752913253663775 2.007752380784761475 0.0000000000000000
-0.0000000000000008 0.0000000000000000 26.8867964278114080

Si Sb
2 2

Direct

0.0000000000000000 0.0000000000000000 0.0438778404244207
0.0000000000000000 0.0000000000000000 0.9561221595755864
0.3333333333333357 0.3333333333333357 0.0895659053972646
0.3333333333333357 0.3333333333333357 0.9104340946027426

POSCAR- β -Si₂Sb₂

1.0000000000000000
3.477529132536688375 -2.007752380784829875 0.0000000000000000
3.47752913253663775 2.007752380784761475 0.0000000000000000
-0.0000000000000008 0.0000000000000000 26.8867964278114080

Si Sb
2 2

Direct

0.0000000000000000 0.0000000000000000 0.0438778404244207
0.0000000000000000 0.0000000000000000 0.9561221595755864
0.3333333333333357 0.3333333333333357 0.0895659053972646
-0.3333333333333357 -0.3333333333333357 0.9104340946027426

POSCAR- α -Si₂Bi₂

4.1000000000000000
0.8798900703605536 -0.5080047689799765 0.0000000000000000
0.8798900703605494 0.5080047689799650 0.0000000000000000
-0.0000000000000001 0.0000000000000000 7.0232546668773681

Si Bi
2 2

Direct

0.0000000000000000 0.0000000000000000 0.0408136768404271
0.0000000000000000 0.0000000000000000 0.9591863231595775
0.3333333333333357 0.3333333333333357 0.0853580790302809
0.3333333333333357 0.3333333333333357 0.9146419209697303

POSCAR- β -Si₂Bi₂

4.1000000000000000
0.8798900703605536 -0.5080047689799765 0.0000000000000000
0.8798900703605494 0.5080047689799650 0.0000000000000000
-0.0000000000000000 0.0000000000000000 7.0232546668773681

Si Bi
2 2

Direct

0.0000000000000000 0.0000000000000000 0.0408136768404271
0.0000000000000000 0.0000000000000000 0.9591863231595775
0.3333333333333357 0.3333333333333357 0.0853580790302809
-0.3333333333333357 -0.3333333333333357 0.9146419209697303

POSCAR- α -Ge₂N₂

1.0000000000000000
2.6858814015117245 -1.550694350172467475 0.0000000000000000
2.685881401511730275 1.5506943501723387 0.0000000000000014
0.0000000000000036 0.0000000000000018 28.7977799986154288

Ge N
2 2

Direct

0.0000000000000000 0.0000000000000000 0.0445360843349821
0.0000000000000000 0.0000000000000000 0.9554639156650027
0.3333333333333357 0.3333333333333357 0.0676387349246264
0.3333333333333357 0.3333333333333357 0.9323612650754014

POSCAR- β -Ge₂N₂

1.0000000000000000
2.6858814015117245 -1.550694350172467475 0.0000000000000000
2.685881401511730275 1.5506943501723387 0.0000000000000014
0.0000000000000036 0.0000000000000018 28.7977799986154288

Ge N
2 2

Direct

0.0000000000000000 0.0000000000000000 0.0445360843349821
0.0000000000000000 0.0000000000000000 0.9554639156650027
0.3333333333333357 0.3333333333333357 0.0676387349246264
-0.3333333333333357 -0.3333333333333357 0.9323612650754014

POSCAR- α -Ge₂P₂

1.0000000000000000
3.17226503600405695 -1.83150807247685755 0.0000000000000000
3.172265036003811375 1.83150807247716285 0.0000000000000000
0.0000000000000000 0.0000000000000000 27.0144259031135050

Ge P
2 2

Direct

0.0000000000000000 0.0000000000000000 0.0463754999822277

0.0000000000000000 0.0000000000000000 0.9536245000177649
0.3333333333333357 0.3333333333333357 0.0860913358014670
0.3333333333333357 0.3333333333333357 0.9139086641985259

POSCAR- β -Ge₂P₂

1.0000000000000000
3.17226503600405695 -1.83150807247685755 0.0000000000000000
3.172265036003811375 1.83150807247716285 0.0000000000000000
0.0000000000000000 0.0000000000000000 27.0144259031135050
Ge P
2 2

Direct

0.0000000000000000 0.0000000000000000 0.0463754999822277
0.0000000000000000 0.0000000000000000 0.9536245000177649
0.3333333333333357 0.3333333333333357 0.0860913358014670
-0.3333333333333357 -0.3333333333333357 0.9139086641985259

POSCAR- α -Ge₂As₂

1.0000000000000000
3.308544491737140725 -1.91018905292791885 0.0000000000000000
3.3085444917368041 1.91018905292809205 0.0000000000000000
0.0000000000000000 0.0000000000000000 24.8348026513106568
Ge As
2 2

Direct

0.0000000000000000 0.0000000000000000 0.0503191959638081
0.0000000000000000 0.0000000000000000 0.9496808040361779
0.3333333333333357 0.3333333333333357 0.0966425407832867
0.3333333333333357 0.3333333333333357 0.9033574592167131

POSCAR- β -Ge₂As₂

1.0000000000000000
3.308544491737140725 -1.91018905292791885 0.0000000000000000
3.3085444917368041 1.91018905292809205 0.0000000000000000
0.0000000000000000 0.0000000000000000 24.8348026513106568
Ge As
2 2

Direct

0.0000000000000000 0.0000000000000000 0.0503191959638081
0.0000000000000000 0.0000000000000000 0.9496808040361779
0.3333333333333357 0.3333333333333357 0.0966425407832867
-0.3333333333333357 -0.3333333333333357 0.9033574592167131

POSCAR- α -Ge₂Sb₂

1.0000000000000000
3.571305899704054975 -2.061894427885734525 -0.0000000000000028
3.57130589870062875 2.0618944265292214 0.0000000000000042
0.0000000000000000 0.0000000000000010 27.9919743476202534
Ge Sb

2 2

Direct

0.0000000000000000	0.0000000000000000	0.0446703061143147
0.0000000000000000	0.0000000000000000	0.9554069217168412
0.3333333333333357	0.3333333333333357	0.0895737796231723
0.3333333333333357	0.3333333333333357	0.9105033723662791

POSCAR- β -Ge₂Sb₂

1.0000000000000000		
3.571305899704054975	-2.061894427885734525	-0.0000000000000028
3.57130589870062875	2.0618944265292214	0.0000000000000042
0.0000000000000000	0.0000000000000010	27.9919743476202534

Ge Sb
2 2

Direct

0.0000000000000000	0.0000000000000000	0.0446703061143147
0.0000000000000000	0.0000000000000000	0.9554069217168412
0.3333333333333357	0.3333333333333357	0.0895737796231723
-0.3333333333333357	-0.3333333333333357	0.9105033723662791

POSCAR- α -Ge₂Bi₂

1.0000000000000000		
3.691898116261825175	-2.131518371244824025	0.0000000000000000
3.691898116261731025	2.131518371244842675	0.0000000000000000
0.0000000000000000	0.0000000000000000	27.2970182528660921

Ge Bi
2 2

Direct

0.0000000000000000	0.0000000000000000	0.0456521176766244
0.0000000000000000	0.0000000000000000	0.9543478823233678
0.3333333333333357	0.3333333333333357	0.0933182337000747
0.3333333333333357	0.3333333333333357	0.9066817662999325

POSCAR- β -Ge₂Bi₂

1.0000000000000000		
3.691898116261825175	-2.131518371244824025	0.0000000000000000
3.691898116261731025	2.131518371244842675	0.0000000000000000
0.0000000000000000	0.0000000000000000	27.2970182528660921

Ge Bi
2 2

Direct

0.0000000000000000	0.0000000000000000	0.0456521176766244
0.0000000000000000	0.0000000000000000	0.9543478823233678
0.3333333333333357	0.3333333333333357	0.0933182337000747
-0.3333333333333357	-0.3333333333333357	0.9066817662999325

POSCAR- α -Sn₂N₂

1.0000000000000000		
2.961570375750981025	-1.709863453663774025	0.0000000000000000

2.961570375750992125 1.709863453663735375 0.0000000000000000
0.0000000000000000 0.0000000000000000 25.4964114750307900

Sn N
2 2

Direct

0.0000000000000000 0.0000000000000000 0.0583626132257341
0.0000000000000000 0.0000000000000000 0.9416373867743063
0.3333333333333357 0.3333333333333357 0.0870608867702451
0.3333333333333357 0.3333333333333357 0.9129391132297298

POSCAR- β -Sn₂N₂

1.0000000000000000

2.961570375750981025 -1.709863453663774025 0.0000000000000000
2.961570375750992125 1.709863453663735375 0.0000000000000000
0.0000000000000000 0.0000000000000000 25.4964114750307900

Sn N
2 2

Direct

0.0000000000000000 0.0000000000000000 0.0583626132257341
0.0000000000000000 0.0000000000000000 0.9416373867743063
0.3333333333333357 0.3333333333333357 0.0870608867702451
-0.3333333333333357 -0.3333333333333357 0.9129391132297298

POSCAR- α -Sn₂P₂

1.0000000000000000

3.4219651314743511 -1.9756724897968343 0.0000000000000000
3.4219651314683488 1.9756724897896818 0.0000000000000000
0.0000000000000000 0.0000000000000000 27.9061349396144713

Sn P
2 2

Direct

0.0000000000000000 0.0000000000000000 0.0517690944281229
0.0000000000000000 0.0000000000000000 0.9482309055718420
0.3333333333333357 0.3333333333333357 0.0935128711615948
0.3333333333333357 0.3333333333333357 0.9064871288381781

POSCAR- β -Sn₂P₂

1.0000000000000000

3.4219651314743511 -1.9756724897968343 0.0000000000000000
3.4219651314683488 1.9756724897896818 0.0000000000000000
0.0000000000000000 0.0000000000000000 27.9061349396144713

Sn P
2 2

Direct

0.0000000000000000 0.0000000000000000 0.0517690944281229
0.0000000000000000 0.0000000000000000 0.9482309055718420
0.3333333333333357 0.3333333333333357 0.0935128711615948
-0.3333333333333357 -0.3333333333333357 0.9064871288381781

POSCAR- α -Sn₂As₂

1.0000000000000000
3.543520771516774025 -2.045852671314388975 0.0000000000000000
3.543520771516788225 2.0458526713143712 0.0000000000000000
0.0000000000000000 0.0000000000000000 29.3994156300147687
Sn As
2 2

Direct

0.0000000000000000 0.0000000000000000 0.0489564718281513
0.0000000000000000 0.0000000000000000 0.9510435281718402
0.3333333333333357 0.3333333333333357 0.0912109207509854
0.3333333333333357 0.3333333333333357 0.9087890792490299

POSCAR- β -Sn₂As₂

1.0000000000000000
3.543520771516774025 -2.045852671314388975 0.0000000000000000
3.543520771516788225 2.0458526713143712 0.0000000000000000
0.0000000000000000 0.0000000000000000 29.3994156300147687
Sn As
2 2

Direct

0.0000000000000000 0.0000000000000000 0.0489564718281513
0.0000000000000000 0.0000000000000000 0.9510435281718402
0.3333333333333357 0.3333333333333357 0.0912109207509854
-0.3333333333333357 -0.3333333333333357 0.9087890792490299

POSCAR- α -Sn₂Sb₂

1.0000000000000000
3.7949779723496051 -2.1910315539079348 0.0000000000000000
3.7949779723491468 2.1910315539066585 0.0000000000000000
0.0000000000000002 0.0000000000000000 28.9659127945051722
Sn Sb
2 2

Direct

0.0000000000000000 0.0000000000000000 0.0507544752408575
0.0000000000000000 0.0000000000000000 0.9517129312883560
0.3333333333333357 0.3333333333333357 0.0976120300719327
0.3333333333333357 0.3333333333333357 0.9048553864335136

POSCAR- β -Sn₂Sb₂

1.0000000000000000
3.7949779723496051 -2.1910315539079348 0.0000000000000000
3.7949779723491468 2.1910315539066585 0.0000000000000000
0.0000000000000002 0.0000000000000000 28.9659127945051722
Sn Sb
2 2

Direct

0.0000000000000000 0.0000000000000000 0.0507544752408575
0.0000000000000000 0.0000000000000000 0.9517129312883560

0.3333333333333357 0.3333333333333357 0.0976120300719327
-0.3333333333333357 -0.3333333333333357 0.9048553864335136

POSCAR- α -Sn₂Bi₂

1.0000000000000000
3.90439686116838035 -2.25420457883116355 0.0000000000000000
3.9043968611661386 2.254204578826708 0.0000000000000000
0.00000000000000003 0.0000000000000000 27.3651496665047489
Sn Bi
2 2

Direct

0.0000000000000000 0.0000000000000000 0.0534734730418469
0.0000000000000000 0.0000000000000000 0.9489939334873496
0.3333333333333357 0.3333333333333357 0.1046120631251983
0.3333333333333357 0.3333333333333357 0.8978553533802553

POSCAR- β -Sn₂Bi₂

1.0000000000000000
3.90439686116838035 -2.25420457883116355 0.0000000000000000
3.9043968611661386 2.254204578826708 0.0000000000000000
0.00000000000000003 0.0000000000000000 27.3651496665047489
Sn Bi
2 2

Direct

0.0000000000000000 0.0000000000000000 0.0534734730418469
0.0000000000000000 0.0000000000000000 0.9489939334873496
0.3333333333333357 0.3333333333333357 0.1046120631251983
-0.3333333333333357 -0.3333333333333357 0.8978553533802553

POSCAR- α -Pb₂N₂

1.0000000000000000
3.152967822486948175 -1.820366821053765575 0.0000000000000000
3.152967822486964175 1.82036682105379265 0.0000000000000000
0.00000000000000000 0.0000000000000000 26.6253221809360312
Pb N
2 2

Direct

0.0000000000000000 0.0000000000000000 0.0596082803201259
0.0000000000000000 0.0000000000000000 0.9403917196798659
0.3333333333333357 0.3333333333333357 0.0892077311039359
0.3333333333333357 0.3333333333333357 0.9107922688960629

POSCAR- β -Pb₂N₂

1.0000000000000000
3.152967822486948175 -1.820366821053765575 0.0000000000000000
3.152967822486964175 1.82036682105379265 0.0000000000000000
0.00000000000000000 0.0000000000000000 26.6253221809360312
Pb N
2 2

Direct

0.0000000000000000	0.0000000000000000	0.0596082803201259
0.0000000000000000	0.0000000000000000	0.9403917196798659
0.3333333333333357	0.3333333333333357	0.0892077311039359
-0.3333333333333357	-0.3333333333333357	0.9107922688960629

POSCAR- α -Pb₂P₂

1.0000000000000000		
3.5664225783782908	-2.05907503567105765	0.0000000000000000
3.566422578378206425	2.059075035670562925	0.0000000000000000
0.0000000000000000	0.0000000000000000	29.0505717665422445

Pb P
2 2

Direct

0.0000000000000000	0.0000000000000000	0.0526436393207049
0.0000000000000000	0.0000000000000000	0.9473563606793014
0.3333333333333357	0.3333333333333357	0.0944879345040668
0.3333333333333357	0.3333333333333357	0.9055120654959324

POSCAR- β -Pb₂P₂

1.0000000000000000		
3.5664225783782908	-2.05907503567105765	0.0000000000000000
3.566422578378206425	2.059075035670562925	0.0000000000000000
0.0000000000000000	0.0000000000000000	29.0505717665422445

Pb P
2 2

Direct

0.0000000000000000	0.0000000000000000	0.0526436393207049
0.0000000000000000	0.0000000000000000	0.9473563606793014
0.3333333333333357	0.3333333333333357	0.0944879345040668
-0.3333333333333357	-0.3333333333333357	0.9055120654959324

POSCAR- α -Pb₂As₂

1.0000000000000000		
3.677677983482954725	-2.1233083737575389	0.0000000000000000
3.677677983482653175	2.1233083737565872	0.0000000000000000
0.0000000000000000	0.0000000000000000	27.3195087628506776

Pb As
2 2

Direct

0.0000000000000000	0.0000000000000000	0.0557389838268677
0.0000000000000000	0.0000000000000000	0.9442610161731174
0.3333333333333357	0.3333333333333357	0.1027734402906814
0.3333333333333357	0.3333333333333357	0.8972265597093336

POSCAR- β -Pb₂As₂

1.0000000000000000		
3.677677983482954725	-2.1233083737575389	0.0000000000000000
3.677677983482653175	2.1233083737565872	0.0000000000000000

0.0000000000000000	0.0000000000000000	27.3195087628506776
Pb As		
2 2		
Direct		
0.0000000000000000	0.0000000000000000	0.0557389838268677
0.0000000000000000	0.0000000000000000	0.9442610161731174
0.3333333333333357	0.3333333333333357	0.1027734402906814
-0.3333333333333357	-0.3333333333333357	0.8972265597093336

POSCAR- α -Pb₂Sb₂

1.0000000000000000		
3.919367253171011975	-2.26284773857625465	0.0000000000000000
3.919367253243375875	2.262847738704010675	0.0000000000000000
0.0000000000000000	0.0000000000000000	27.7386661521943836
Pb Sb		
2 2		

Direct

0.0000000000000000	0.0000000000000000	0.0547209410739452
0.0000000000000000	0.0000000000000000	0.9452790589260548
0.3333333333333357	0.3333333333333357	0.1048009881253003
0.3333333333333357	0.3333333333333357	0.8951990118746931

POSCAR- β -Pb₂Sb₂

1.0000000000000000		
3.919367253171011975	-2.26284773857625465	0.0000000000000000
3.919367253243375875	2.262847738704010675	0.0000000000000000
0.0000000000000000	0.0000000000000000	27.7386661521943836
Pb Sb		
2 2		

Direct

0.0000000000000000	0.0000000000000000	0.0547209410739452
0.0000000000000000	0.0000000000000000	0.9452790589260548
0.3333333333333357	0.3333333333333357	0.1048009881253003
-0.3333333333333357	-0.3333333333333357	0.8951990118746931

POSCAR- α -Pb₂Bi₂

1.0000000000000000		
4.009153338919828625	-2.314685759449021325	0.0000000000000000
4.009153338919734475	2.3146857594469621	0.0000000000000000
0.0000000000000000	0.0000000000000000	31.1987269062439410
Pb Bi		
2 2		

Direct

0.0000000000000000	0.0000000000000000	0.0483810534543669
0.0000000000000000	0.0000000000000000	0.9516189465456331
0.3333333333333357	0.3333333333333357	0.0943381093385243
0.3333333333333357	0.3333333333333357	0.9056618906615963

POSCAR- β -Pb₂Bi₂

1.0000000000000000		
4.009153338919828625	-2.314685759449021325	0.0000000000000000
4.009153338919734475	2.3146857594469621	0.0000000000000000
0.0000000000000000	0.0000000000000000	31.1987269062439410

Pb	Bi
2	2

Direct

0.0000000000000000	0.0000000000000000	0.0483810534543669
0.0000000000000000	0.0000000000000000	0.9516189465456331
0.3333333333333357	0.3333333333333357	0.0943381093385243
-0.3333333333333357	-0.3333333333333357	0.9056618906615963

References

1. Jiesen Li, Wanxing Lin, Junjun Shi, Feng Zhu, Weiliang Wang, Haiwen Xie, Dao-Xin Yao, Novel Phases of Semi-Conducting Silicon Nitride Bilayer: A First-Principle Study, arXiv:1707.02819